# Che cos’è un geotermobarometro?

# Che cos'è un geotermobarometro?

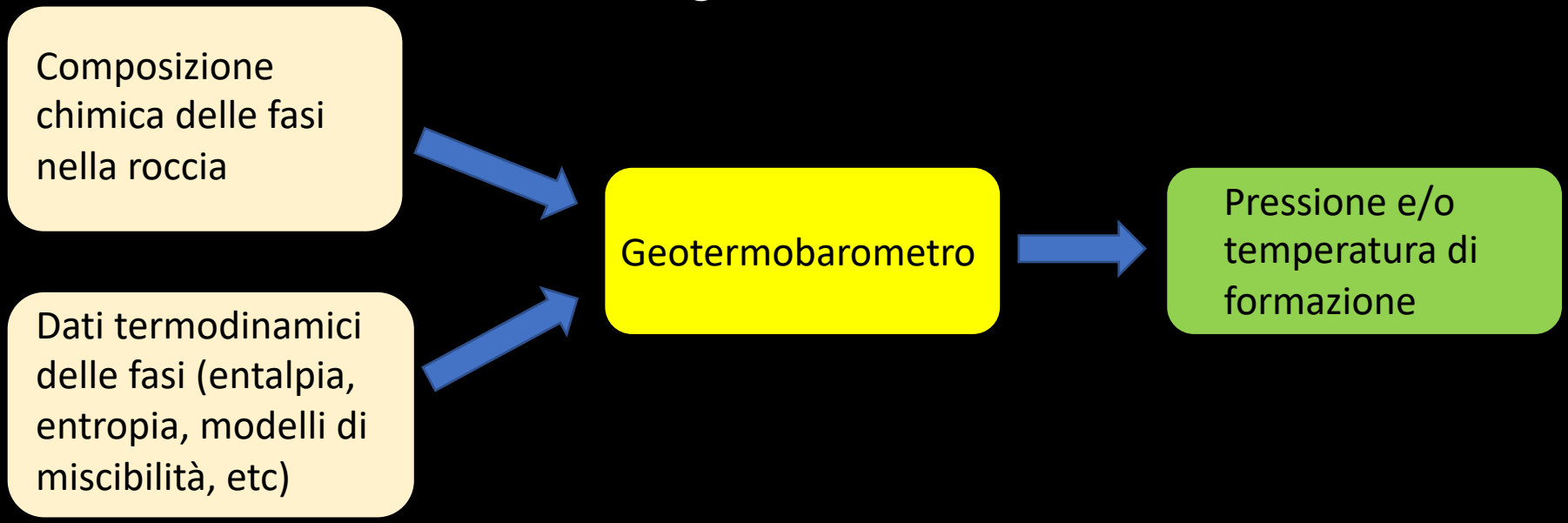

# Che cos'è un geotermobarometro?

Composizione chimica delle fasi nella roccia

Dati termodinamici delle fasi (entalpia, entropia, modelli di miscibilità, etc)

Geotermobarometro

*(Sistema di uno o più equazioni non lineari)*

Pressione e/o temperatura di formazione

$$\Delta H_e + T\,\Delta S_e + \boldsymbol{P}\,\Delta V_e + RT ln K_e = 0$$

$$K_e = \prod j \left(\gamma_j X_j\right)^{\nu_j}$$

$\gamma_j$= coefficiente di attività

$X_j$= frazione molare (composizione chimica)

$\nu_j$= coefficiente stechiometrico

Esempio di equilibrio di fase (*e*) con *j* end-members:

$Mg_2Si_2O_6$ + $NaAlSi_2O_6$ = $Mg_2SiO_4$ + $NaAlSi_3O_8$

| enstatite | jadeite | forsterite | albite |
|---|---|---|---|
| *(pirosseno)* | *(pirosseno)* | *(olivina)* | *(plagioclasio)* |

# A cosa serve?

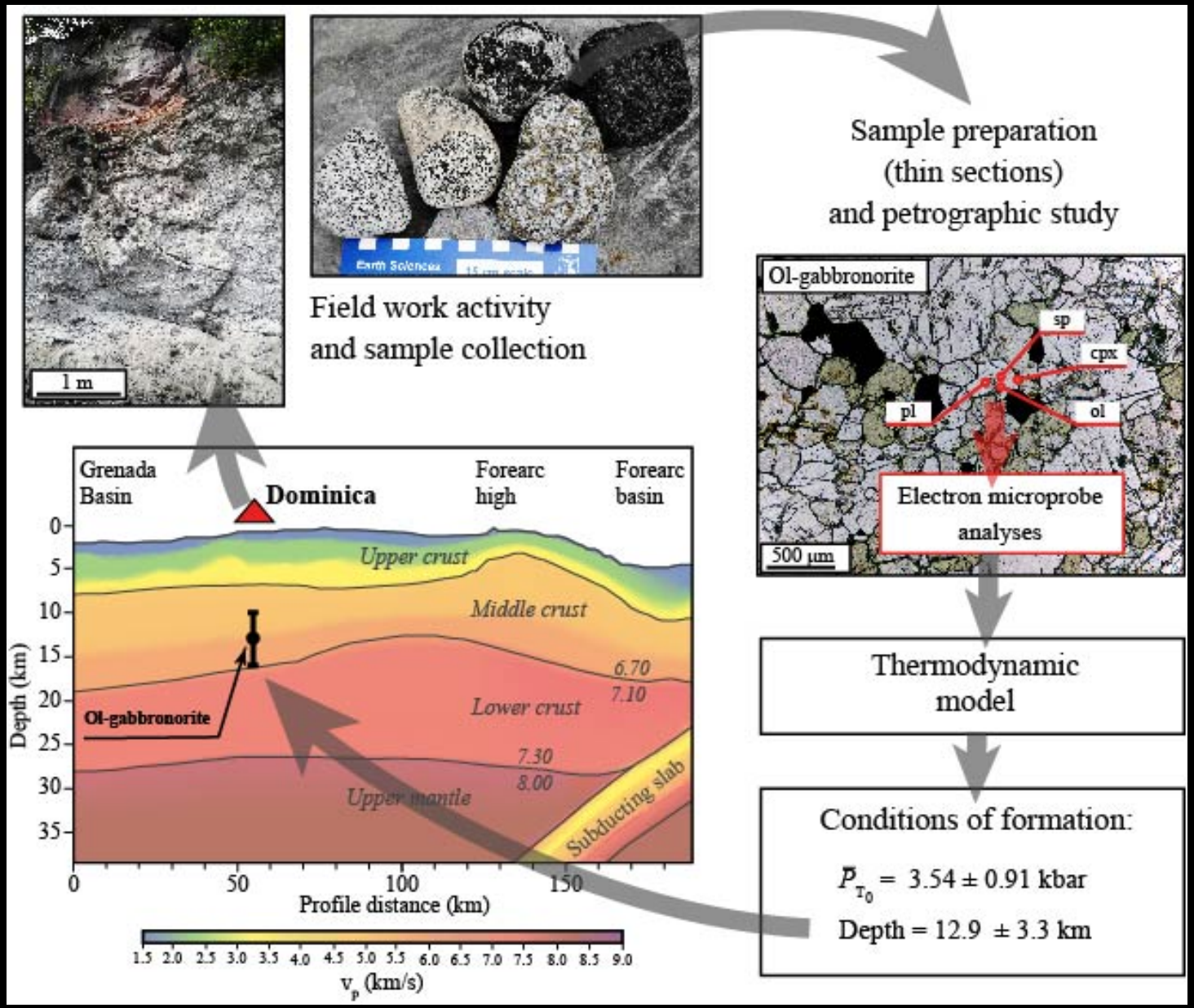
1 m
Field work activity
and sample collection
Sample preparation
(thin sections)
and petrographic study
Ol-gabbronorite
sp
cpx
pl
ol
Electron microprobe
analyses
500 µm
Grenada
Basin
Dominica
Forearc
high
Forearc
basin
Upper crust
Middle crust
Lower crust
Upper mantle
6.70
7.10
7.30
8.00
Ol-gabbronorite
Subducting slab
Depth (km)
0
5
10
15
20
25
30
35
0
50
100
150
Profile distance (km)
1.5 2.0 2.5 3.0 3.5 4.0 4.5 5.0 5.5 6.0 6.5 7.0 7.5 8.0 8.5 9.0
$v_p$ (km/s)
Thermodynamic
model
Conditions of formation:
$\bar{P}_{T_0}$ = 3.54 ± 0.91 kbar
Depth = 12.9 ± 3.3 km

# UNA BUONA NOTIZIA:

Alcuni geotermobarometri, sebbene basati sulla termodinamica, sono degli algoritmi più semplificati rispetto alle equazioni che vi ho mostrato finora.

In vari casi, gli algoritmi sono molto semplici, ad esempio:

$$T_{\text{Ca-in-opx}}(\text{K}) = \frac{6425 + 26{\cdot}4P}{-\ln \text{Ca}^{\text{opx}} + 1{\cdot}843}$$

*Brey & Köhler (1990; J Pet)*

$$T\,(^{\circ}\text{C}) = \frac{10\,000}{0.512 + 0.873Y_{\text{Cr}} - 0.91\ln(K_{\text{D}})} - 273$$

where $Y_{\text{Cr}} = \text{Cr}/(\text{Cr} + \text{Al})$ in spinel in atomic proportions and $K_{\text{D}} = \text{Al}_2\text{O}_3^{\text{ol}}/\text{Al}_2\text{O}_3^{\text{sp}}$ in wt%

*Wan et al. (2008; Am Min)*

In altri, sono rappresentati da una o più equazioni (relativamente poco complesse) e sono già disponibili e ‘pronti all’uso’ (tramite software come Excel, Matlab, Python, etc).

University of BRISTOL

NERC SCIENCE OF THE ENVIRONMENT

BGI Bayerisches Geoinstitut

# The depth of igneous cumulates in the Lesser Antilles island arc


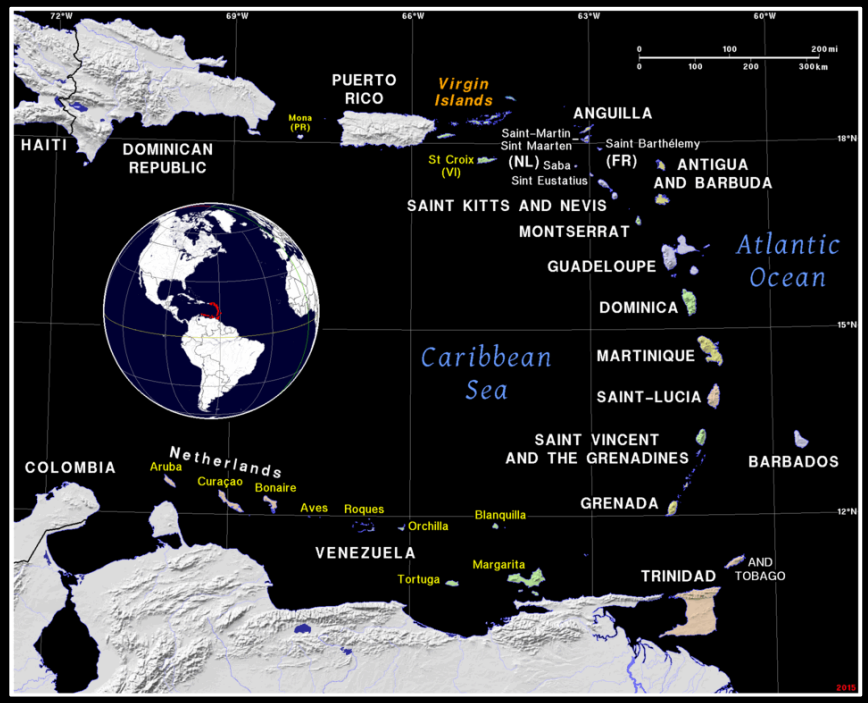


http://ian.macky.net/pat

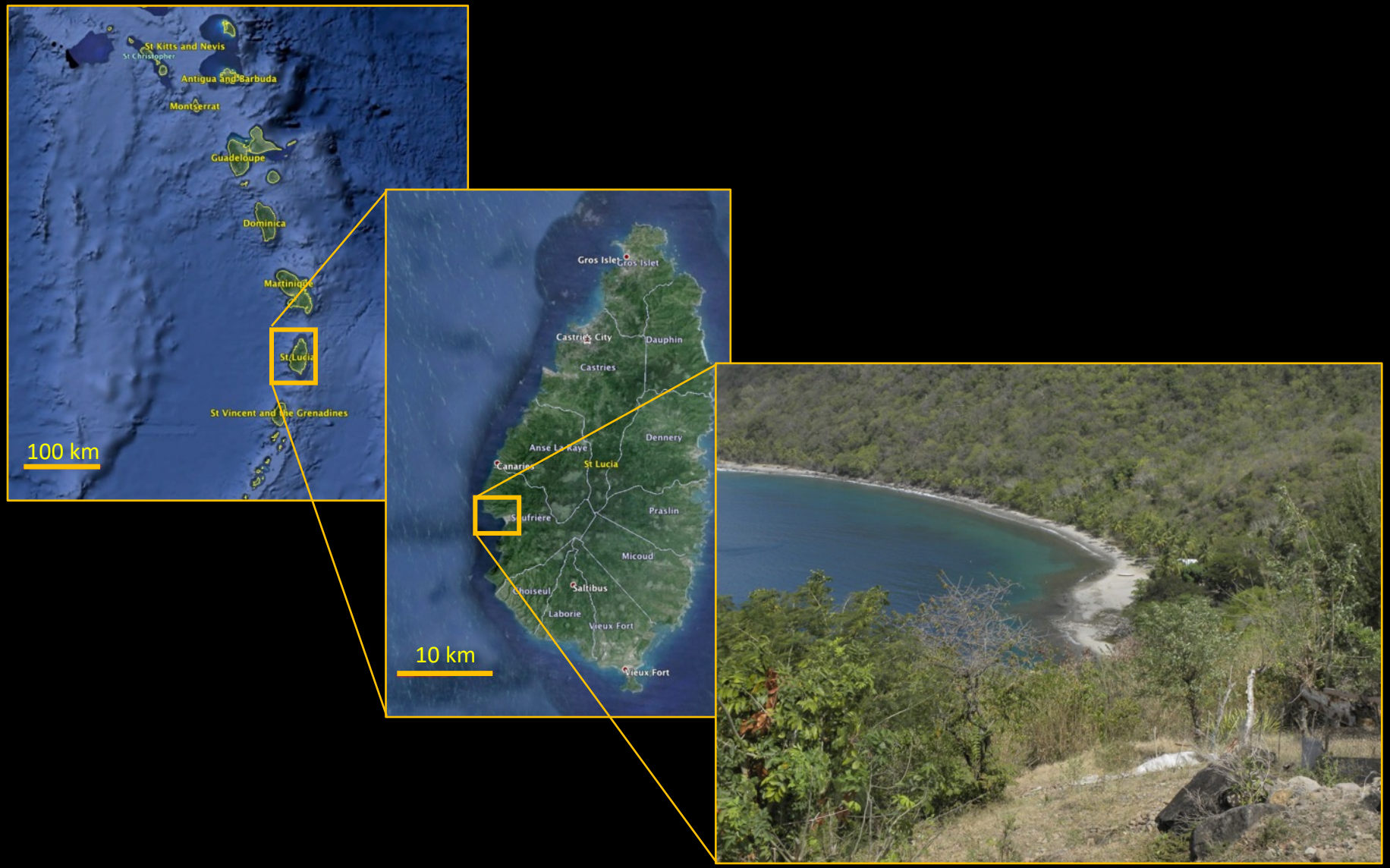
St Kitts and Nevis
St Christopher
Antigua and Barbuda
Montserrat
Guadeloupe
Dominica
Martinique
St Lucia
St Vincent and the Grenadines
100 km
Gros Islet
Castries City
Dauphin
Castries
Dennery
Anse La Raye
Canaries
St Lucia
Soufriere
Praslin
Micoud
Choiseul
Saltibus
Laborie
Vieux Fort
10 km

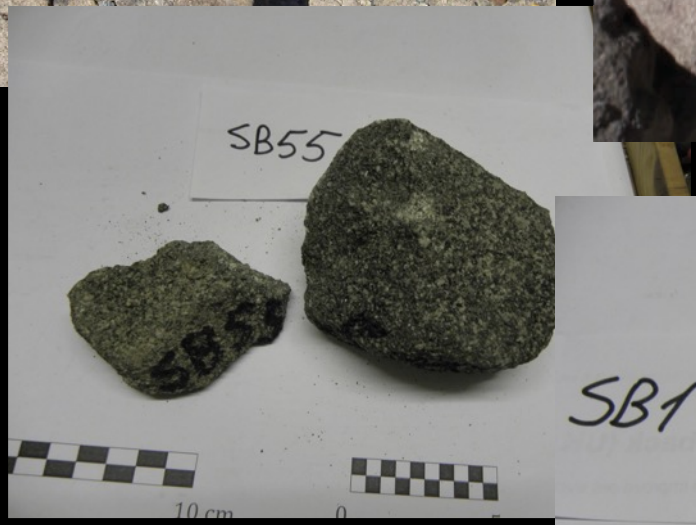
SB55
10 cm


SB17
0
5 cm

# The Lesser Antilles island arc

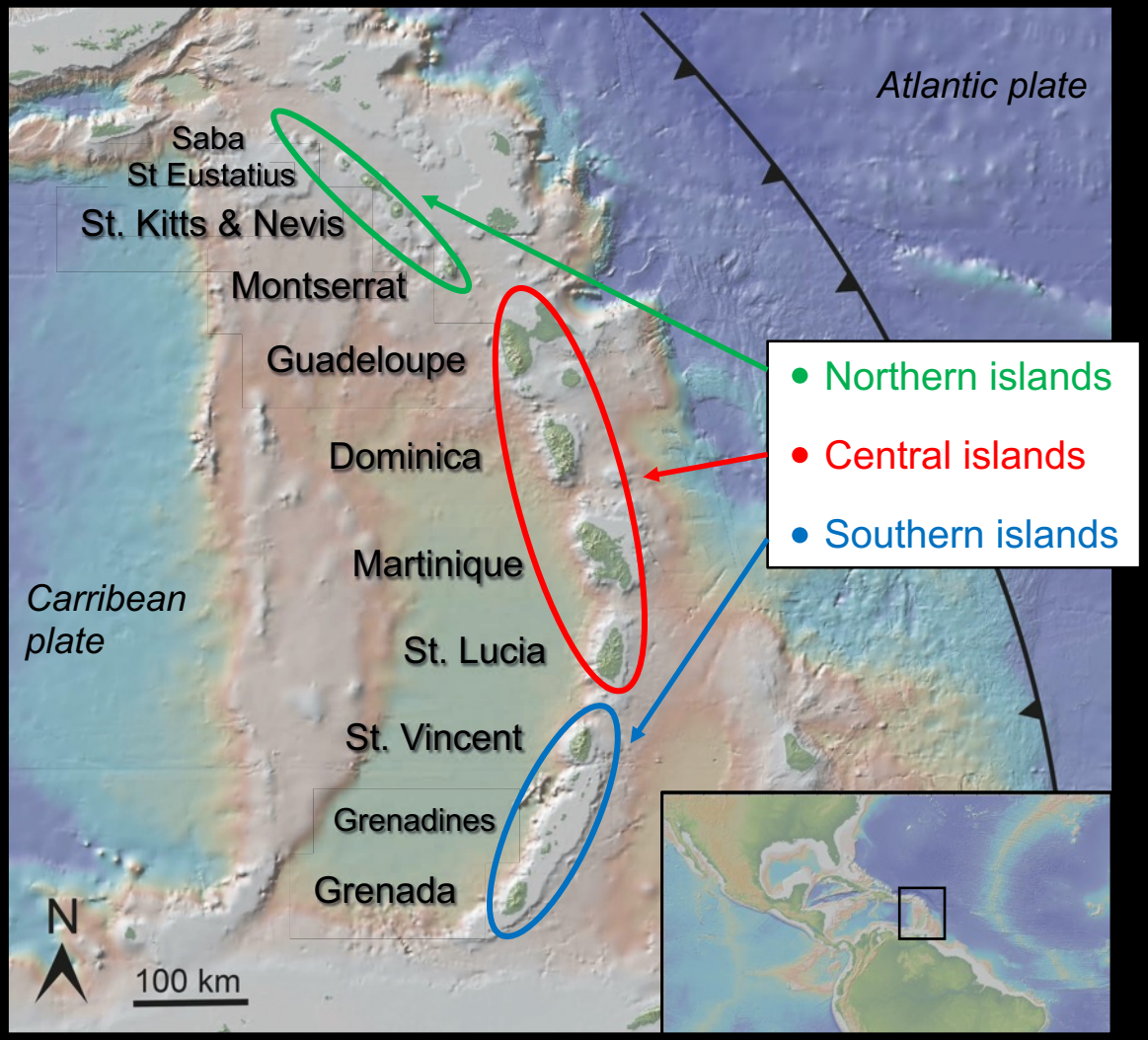


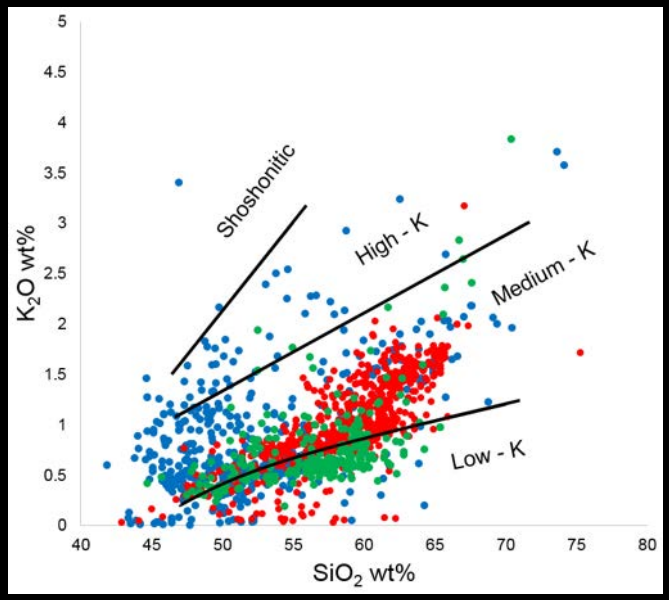


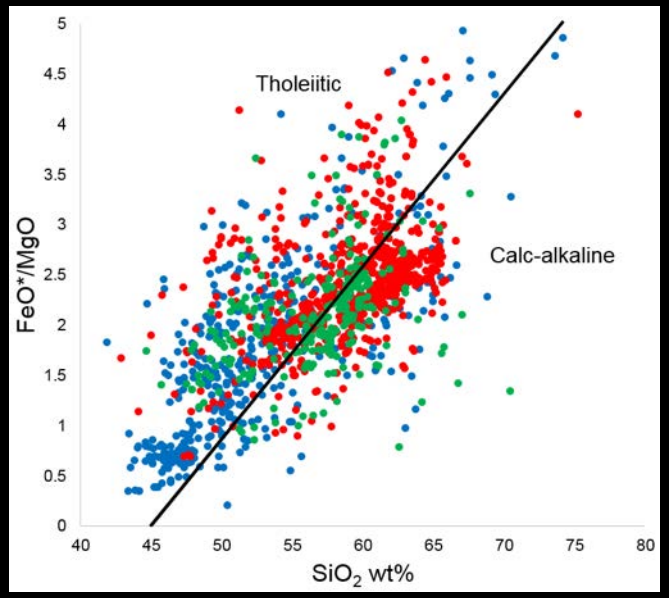

# Plutonic xenoliths


# Petrography of the xenoliths

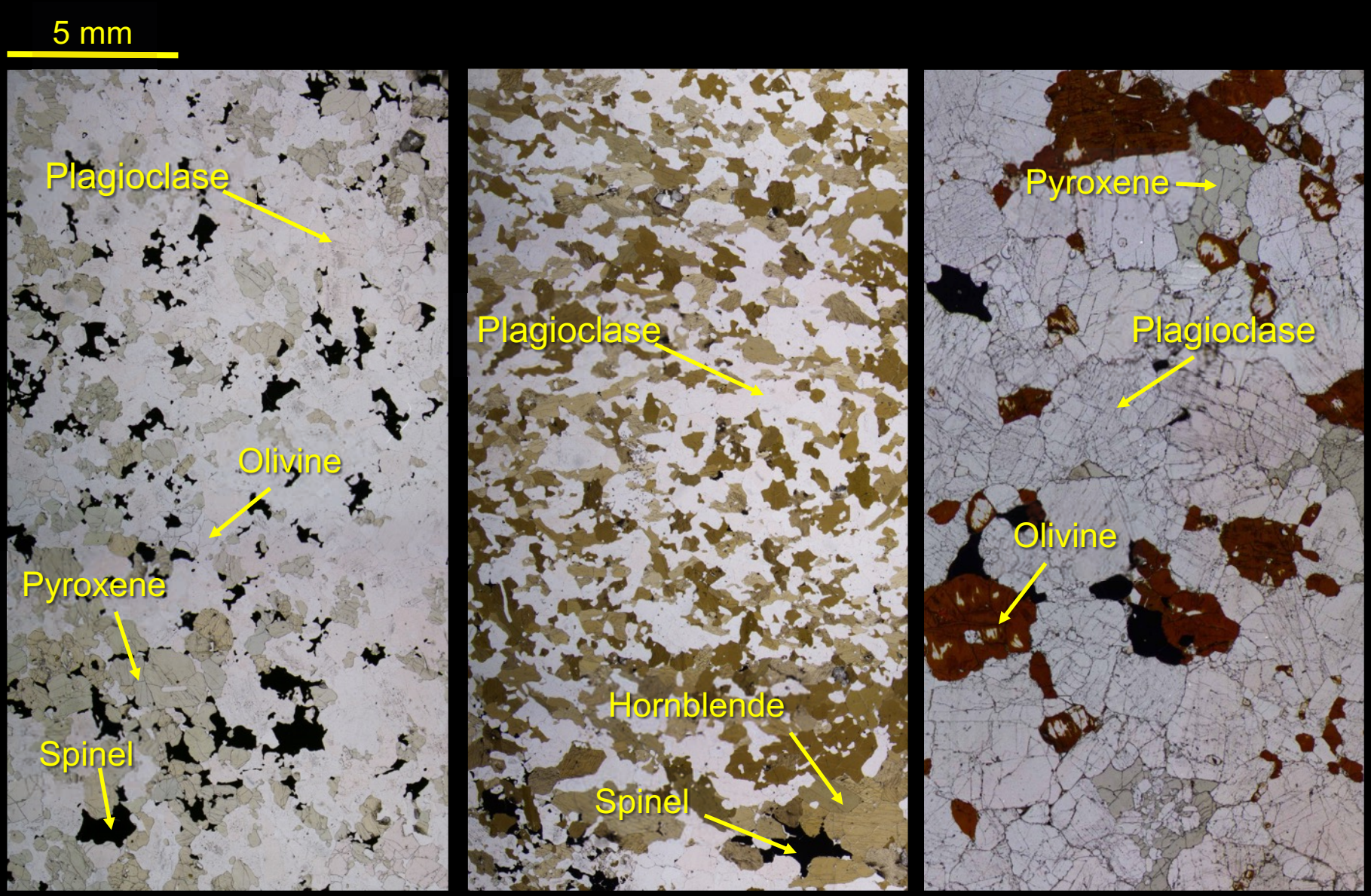

# Geochemistry and mineral chemistry

Bulk rock chemistry:

- consistent with cumulate origin

- suggest fractional crystallization from magmas related to the erupted volcanics

Plagioclase: $An_{75} – An_{98}$

Olivine: $Fo_{60} – Fo_{82}$

Clinopyroxene: augites with mg# = 60 – 92

Spinel: magnetites and minor spinel s.s.

Amphibole: magnesio-hastingsite
magnesio-hornblende

*Martinique*, bulk rock analyses

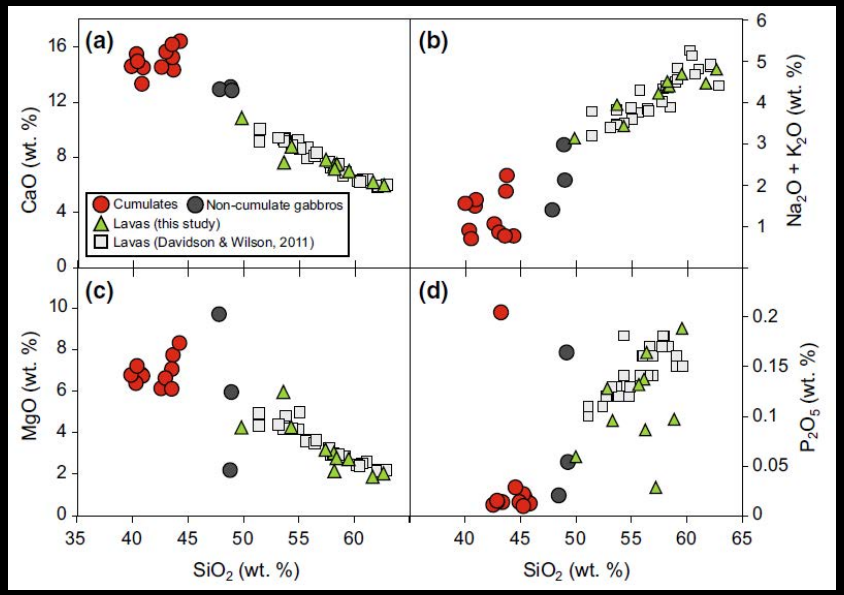


*Cooper et al (2016, CMP)*

All islands, olivine and plagioclase

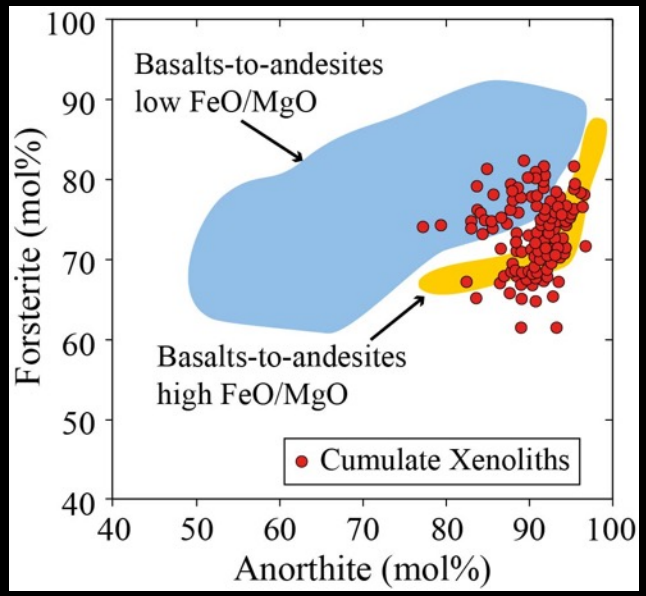

# Pressure estimates

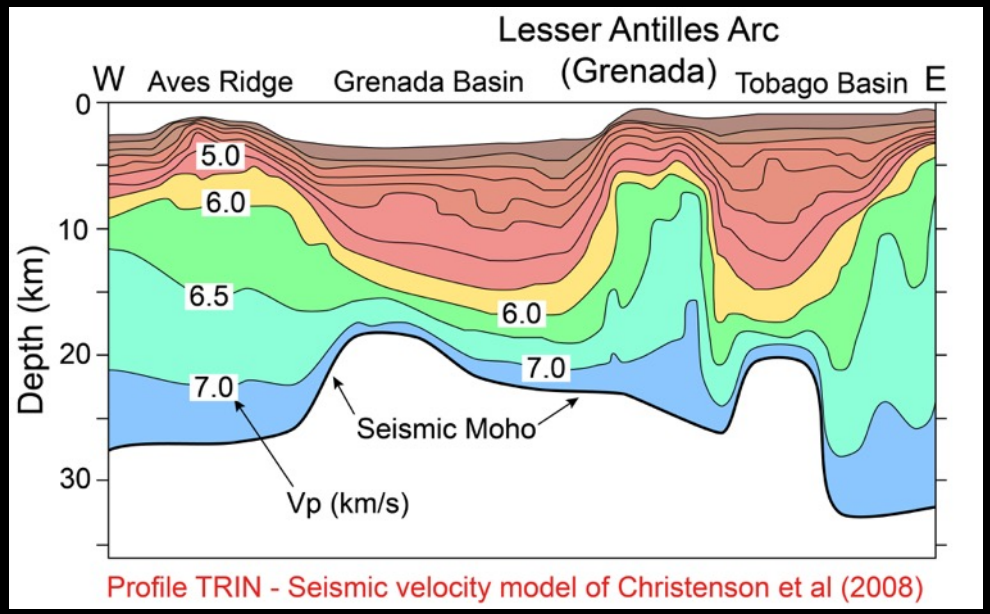

Profile TRIN - Seismic velocity model of Christenson et al (2008)

Which methods are suitable for mafic/ultramafic cumulate rocks?

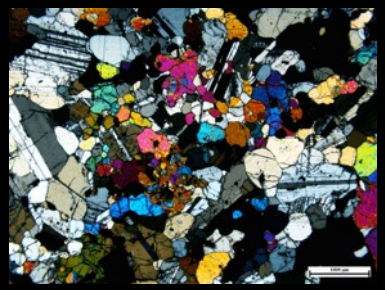

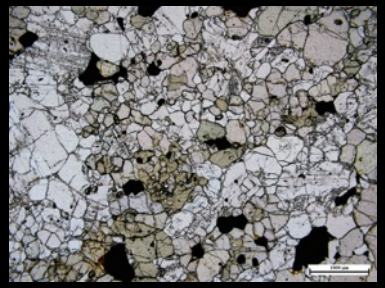

| Method | Uncertainties | Main issues |
|---|---|---|
| Cpx-Opx<br>(e.g., Putirka 2008) | ± 2.8 kbar | • large uncertainties<br>• only few samples have cpx |
| Amph-plag<br>(e.g., Molina et al 2015) | ± 2.3 kbar | • systematic deviations from experiments |
| Cpx-melt<br>(e.g., Neave & Putirka 2017) | ± 1.4 kbar | • only few samples with equilibrium melt<br>• not reliable when T < 1100°C |
| Single cpx<br>(e.g., Putirka 2008) | ± 3.1 kbar | • large uncertainties<br>• likely dependent on composition |
| Single amph<br>(e.g., Ridolfi & Renzulli 2012) | ± 1.1 kbar?<br>± 4.3 kbar? | • likely dependent on composition |

# Single-reaction geothermobarometry

R1) $Mg_2Si_2O_6$ + $CaAl_2SiO_6$ = $Mg_2SiO_4$ + $CaAl_2Si_2O_8$
*c-enstatite* *Ca-tcherm.* *forsterite* *anorthite*

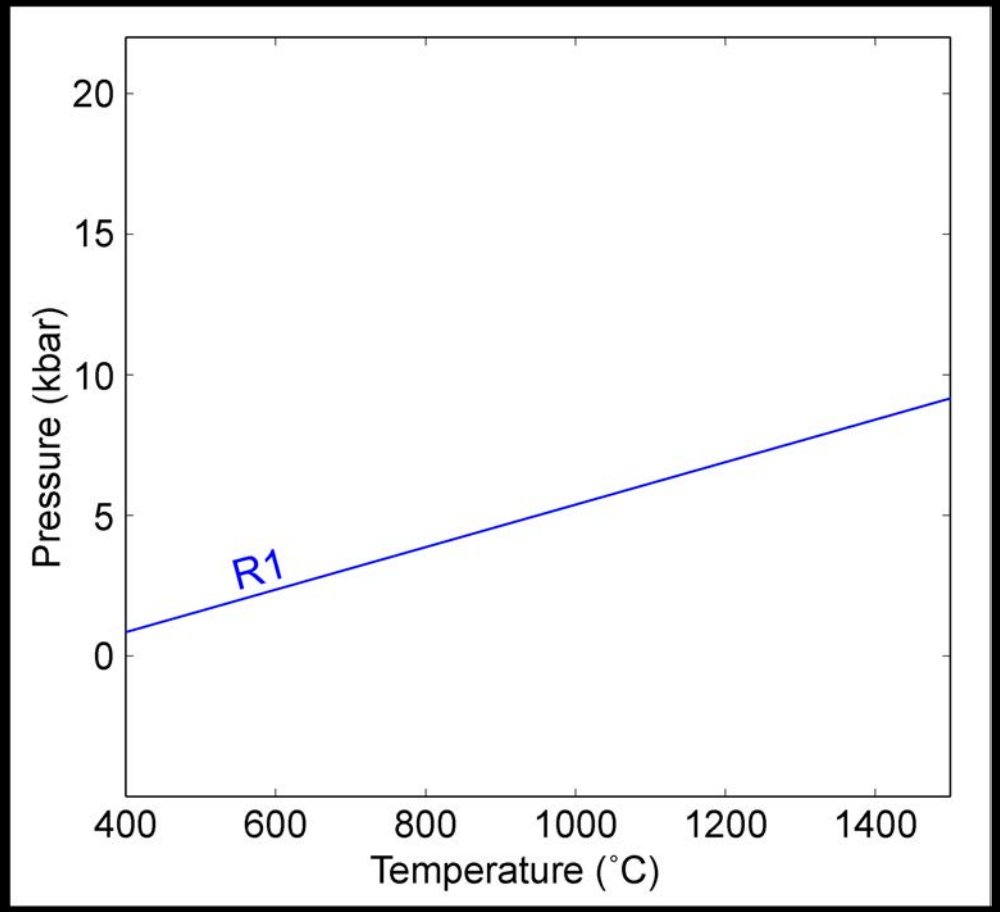


$$\Delta G_1 = \Delta G^0_1 + R\,T\,\ln K_1$$

$$\Delta G^0_1 = \Delta H^0_1 - T\,\Delta S^0_1 + P\,\Delta V^0_1$$

$$K_1 = \frac{a_{Mg2SiO4}\; a_{CaAl2Si2O8}}{a_{Mg2Si2O6}\; a_{CaAl2SiO6}}$$

R1) $\Delta G^0_1 + R\,T\,\ln K_1 = 0$

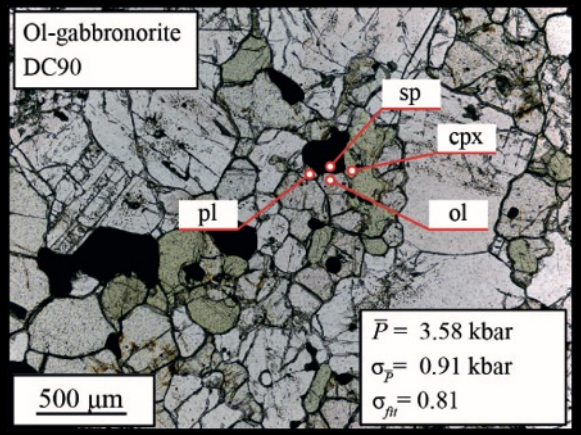

# Multiple-reaction geothermobarometry (e.g., average P method)

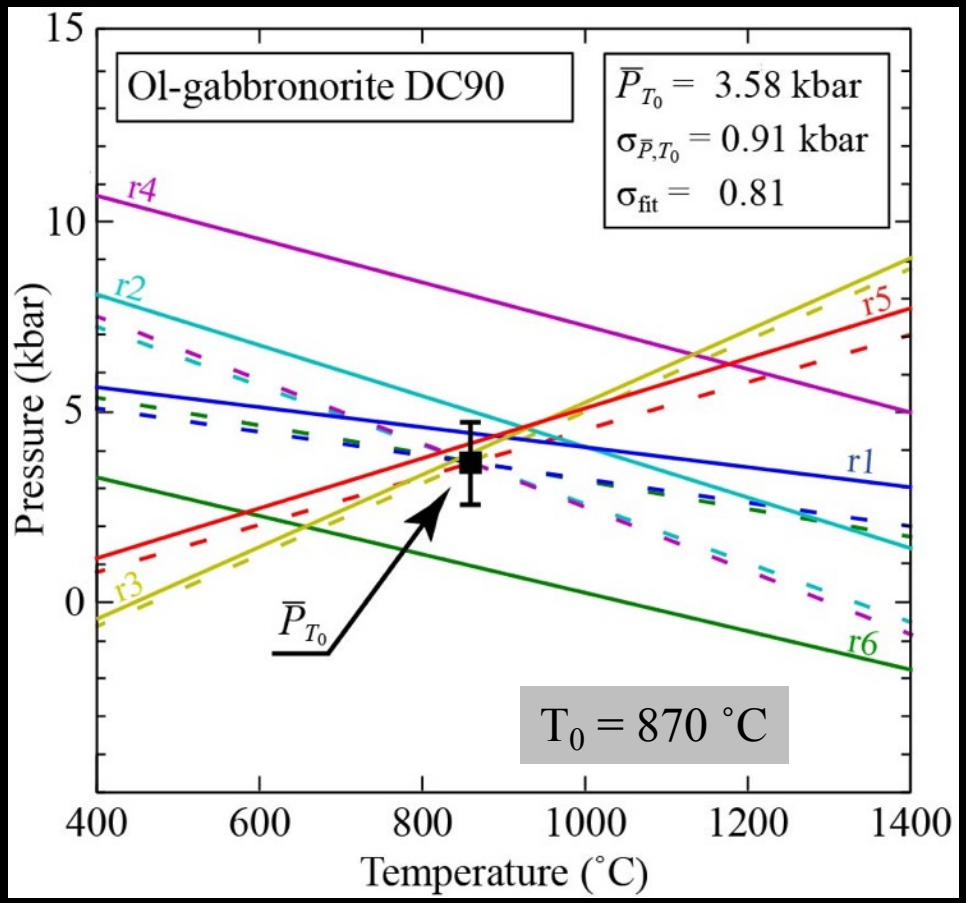


r1) $Mg_2Si_2O_6 + CaAl_2SiO_6 = Mg_2SiO_4 + CaAl_2Si_2O_8$

r2) $Fe_2Si_2O_6 + CaAl_2SiO_6 = Fe_2SiO_4 + CaAl_2Si_2O_8$

r3) $Mg_2Si_2O_6 + NaAlSi_2O_6 = Mg_2SiO_4 + NaAlSi_3O_8$

r4) $Mg_2Si_2O_6 + 2\ CaAl_2SiO_6 = CaMgSi_2O_6 + CaAl_2Si_2O_8 + MgAl_2O_4$

r5) $Mg_2Si_2O_6 + NaAlSi_2O_6 + 2\ FeAl_2O_4 = Fe_2SiO_4 + NaAlSi_3O_8 + 2\ MgAl_2O_4$

r6) $2\ Fe_2Si_2O_6 + 2\ NaFeSi_2O_6 + FeAl_2O_4 = 2\ Fe_2SiO_4 + 2\ NaAlSi_3O_8 + Fe_3O_4$

**Average P takes into account:**

- uncertainties
  - i) analytical errors
  - ii) activity-composition relations
  - iii) thermodynamic properties of pure end-members
- correlations

The positions of the reactions in P-T space are correlated (they share end-members)

**The solution is found when:**

- The reactions are consistent
- The residuals of the activities and enthalpies are minimized

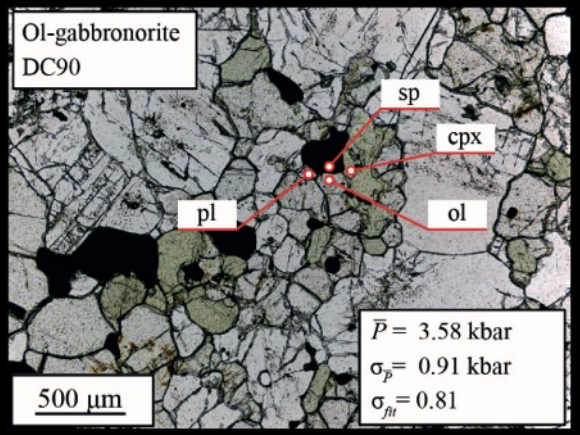

# Application of avP to the experimental samples

Chemical composition of synthetic phases

Thermodynamic data (enthalpy, entropy, interaction parameters)

Temperature

Average P method

Pressure

# Application of avP to the experimental samples

Chemical composition of synthetic phases

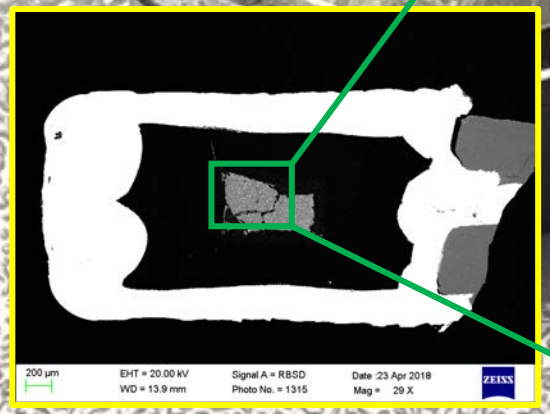


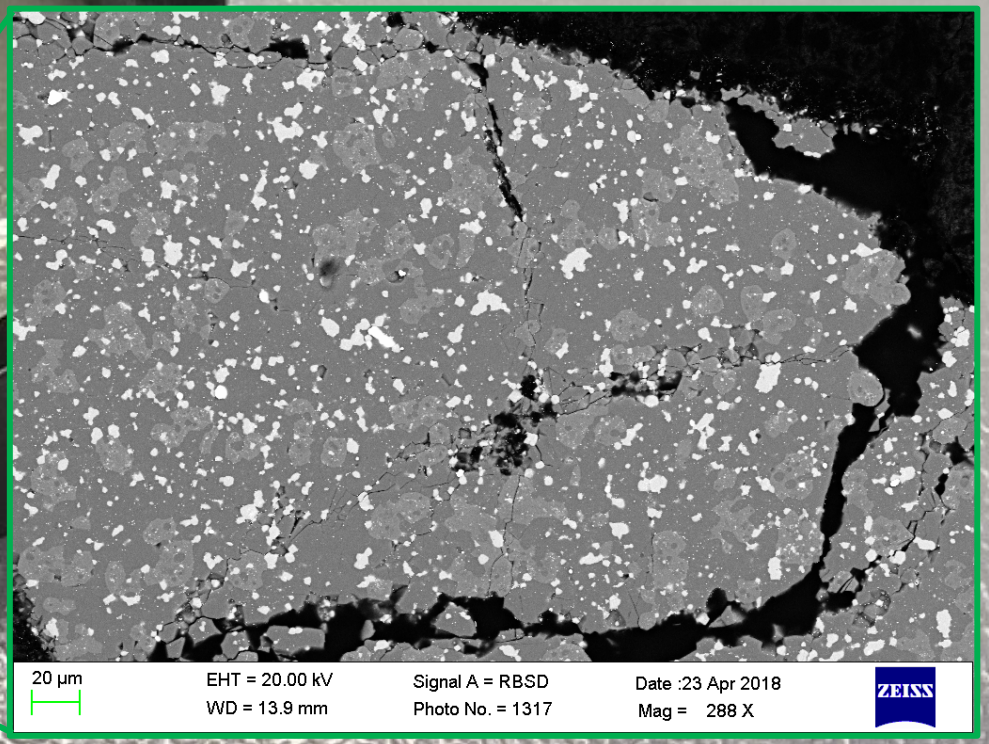

# Application of avP to the experimental samples

Thermodynamic data (enthalpy, entropy, interaction parameters)

*Holland & Powell (2011; J M G)*



**Table 2a.** Molar thermodynamic properties (units: kJ, K, kbar) of the end-members whose formulae can be found in Table 1.

| Group | End-member | $\Delta_f H$ | $\sigma(\Delta_f H)$ | $S$ | $V$ | $C_P$ | | | | $\alpha\kappa$ | | | | $\ell$ |
|---|---|---|---|---|---|---|---|---|---|---|---|---|---|---|
| | | | | | | a | b | c | d | $\alpha_0$ | $\kappa_0$ | $\kappa_0'$ | $\kappa_0''$ | |
| Garnet and olivine | Almandine (alm) | −5260.65 | 1.31 | 342.00 | 11.525 | 0.6773 | 0 | −3772.7 | −5.0440 | 2.12 | 1900.0 | 2.98 | −0.0016 | |
| | Andradite (andr) | −5769.08 | 1.56 | 316.40 | 13.204 | 0.6386 | 0 | −4955.1 | −3.9892 | 2.86 | 1588.0 | 5.68 | −0.0036 | |
| | grossular (gr) | −6642.95 | 1.46 | 255.00 | 12.535 | 0.6260 | 0 | −5779.2 | −4.0029 | 2.20 | 1720.0 | 5.53 | −0.0032 | |
| | Knorringite (knor) | −5687.75 | 3.88 | 317.00 | 11.738 | 0.6130 | 0.3606 | −4178.0 | −3.7294 | 2.37 | 1743.0 | 4.05 | −0.0023 | |
| | Majorite (maj) | −6050.33 | 9.62 | 255.20 | 11.457 | 0.7136 | −0.0997 | −1158.2 | −6.6223 | 1.83 | 1600.0 | 4.56 | −0.0028 | |
| | Pyrope (py) | −6282.13 | 1.06 | 269.50 | 11.313 | 0.6335 | 0 | −5196.1 | −4.3152 | 2.37 | 1743.0 | 4.05 | −0.0023 | |
| | Spessartine (spss) | −5693.65 | 3.14 | 335.30 | 11.792 | 0.6469 | 0 | −4525.8 | −4.4528 | 2.27 | 1740.0 | 6.68 | −0.0038 | |
| | Clinohumite (chum) | −9609.82 | 2.49 | 443.00 | 19.785 | 1.0700 | −1.6533 | −7899.6 | −7.3739 | 2.91 | 1194.0 | 4.79 | −0.0040 | |
| | Fayalite (fa) | −1477.74 | 0.68 | 151.00 | 4.631 | 0.2011 | 1.7330 | −1960.6 | −0.9009 | 2.82 | 1256.0 | 4.68 | −0.0037 | |
| | Forsterite (fo) | −2172.57 | 0.57 | 95.10 | 4.366 | 0.2333 | 0.1494 | −603.8 | −1.8697 | 2.85 | 1285.0 | 3.84 | −0.0030 | |
| | Larnite (lrn) | −2307.04 | 0.90 | 127.60 | 5.160 | 0.2475 | −0.3206 | 0 | −2.0519 | 2.90 | 985.0 | 4.07 | −0.0041 | 1 |
| | Monticellite (mont) | −2251.31 | 0.52 | 109.50 | 5.148 | 0.2507 | −1.0433 | −797.2 | −1.9961 | 2.87 | 1134.0 | 3.87 | −0.0034 | |
| | Tephroite (teph) | −1733.95 | 1.05 | 155.90 | 4.899 | 0.2196 | 0 | −1292.7 | −1.3083 | 2.86 | 1256.0 | 4.68 | −0.0037 | |
| Aluminosilicates | Andalusite (and) | −2588.72 | 0.68 | 92.70 | 5.153 | 0.2773 | −0.6588 | −1914.1 | −2.2656 | 1.81 | 1442.0 | 6.89 | −0.0048 | |
| | Kyanite (ky) | −2593.02 | 0.67 | 83.50 | 4.414 | 0.2794 | −0.7124 | −2055.6 | −2.2894 | 1.92 | 1601.0 | 4.05 | −0.0025 | |
| | Sillimanite (sill) | −2585.85 | 0.68 | 95.40 | 4.986 | 0.2802 | −0.6900 | −1375.7 | −2.3994 | 1.12 | 1640.0 | 5.06 | −0.0031 | 2 |
| | Mullite (amul) | −2485.51 | 0.91 | 113.00 | 5.083 | 0.2448 | 0.0968 | −2533.3 | −1.6416 | 1.36 | 1740.0 | 4.00 | −0.0023 | |
| | Mullite (smul) | −2569.28 | 0.69 | 101.50 | 4.987 | 0.2802 | −0.6900 | −1375.7 | −2.3994 | 1.36 | 1740.0 | 4.00 | −0.0023 | |
| | Chloritoid (fctd) | −3208.31 | 0.80 | 167.00 | 6.980 | 0.4161 | −0.3477 | −2835.9 | −3.3603 | 2.80 | 1456.0 | 4.06 | −0.0028 | |
| | Chloritoid (mctd) | −3549.31 | 0.75 | 146.00 | 6.875 | 0.4174 | −0.3771 | −2920.6 | −3.4178 | 2.63 | 1456.0 | 4.06 | −0.0028 | |
| | Chloritoid (mnctd) | −3336.20 | 1.68 | 166.00 | 7.175 | 0.4644 | −1.2654 | −1147.2 | −4.3410 | 2.60 | 1456.0 | 4.06 | −0.0028 | |
| | Staurolite (fst) | −23 755.04 | 6.34 | 1010.00 | 44.880 | 2.8800 | −5.6595 | −10642.0 | −25.3730 | 1.83 | 1800.0 | 4.76 | −0.0026 | |
| | Staurolite (mnst) | −24 246.42 | 8.60 | 1034.00 | 45.460 | 2.8733 | −8.9064 | −12688.0 | −24.7490 | 2.09 | 1800.0 | 4.76 | −0.0026 | |
| | Staurolite (mst) | −25 124.32 | 6.28 | 910.00 | 44.260 | 2.8205 | −5.9366 | −13774.0 | −24.1260 | 1.81 | 1684.0 | 4.05 | −0.0024 | |
| | Topaz (tpz) | −2900.76 | 0.96 | 100.50 | 5.339 | 0.3877 | −0.7120 | −857.2 | −3.7442 | 1.57 | 1315.0 | 4.06 | −0.0031 | |

# Application of avP to the experimental samples

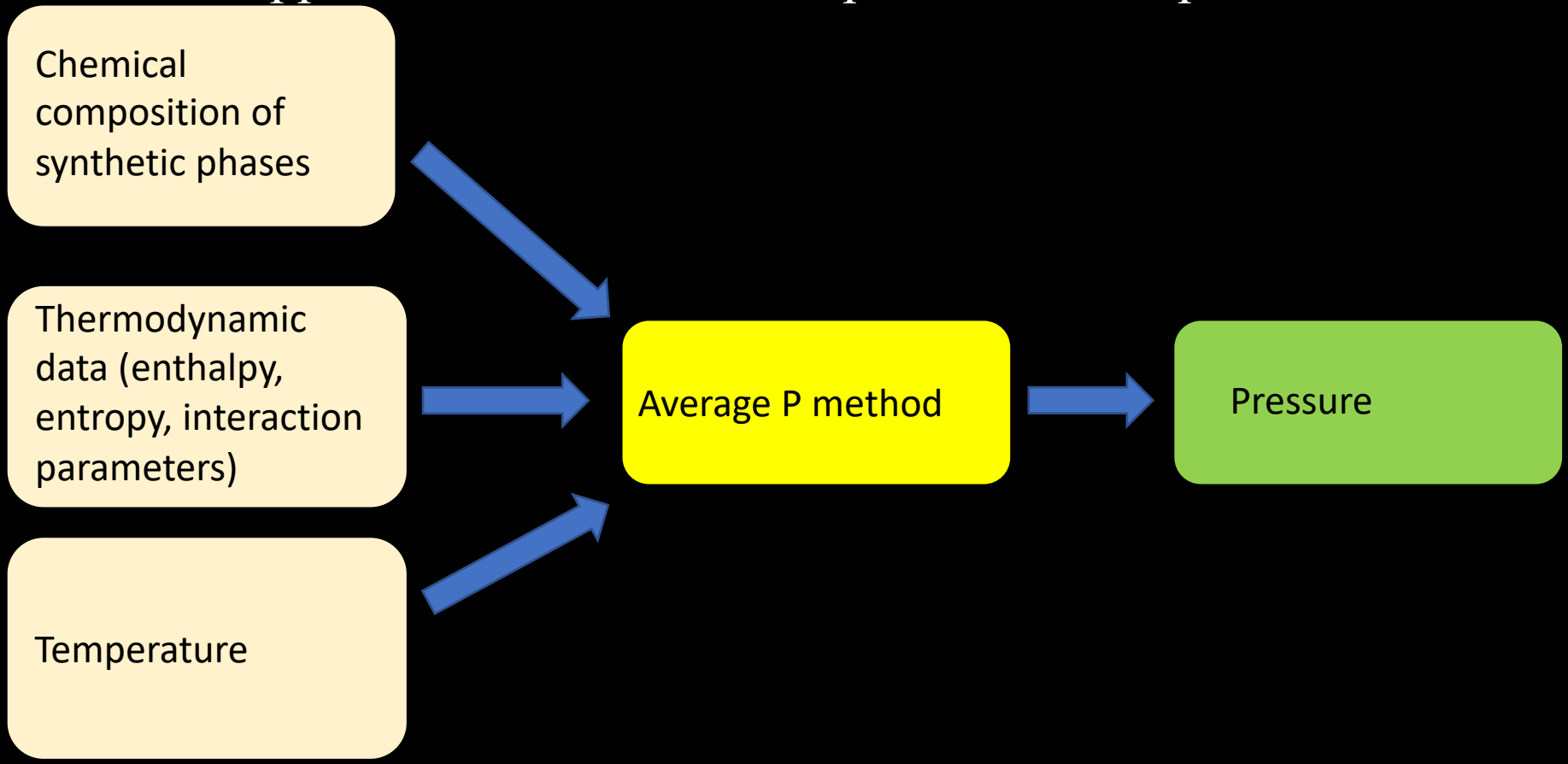

# Application of avP to the experimental samples

Tested on: phase equilibrium experiments in andesitic, basaltic and peridotitic systems

P-T range: P = 0.5 – 9.5 kbar; T = 950 – 1250 ºC

Equilibria: **Spinel + Clinopyroxene + Olivine + Plagioclase**

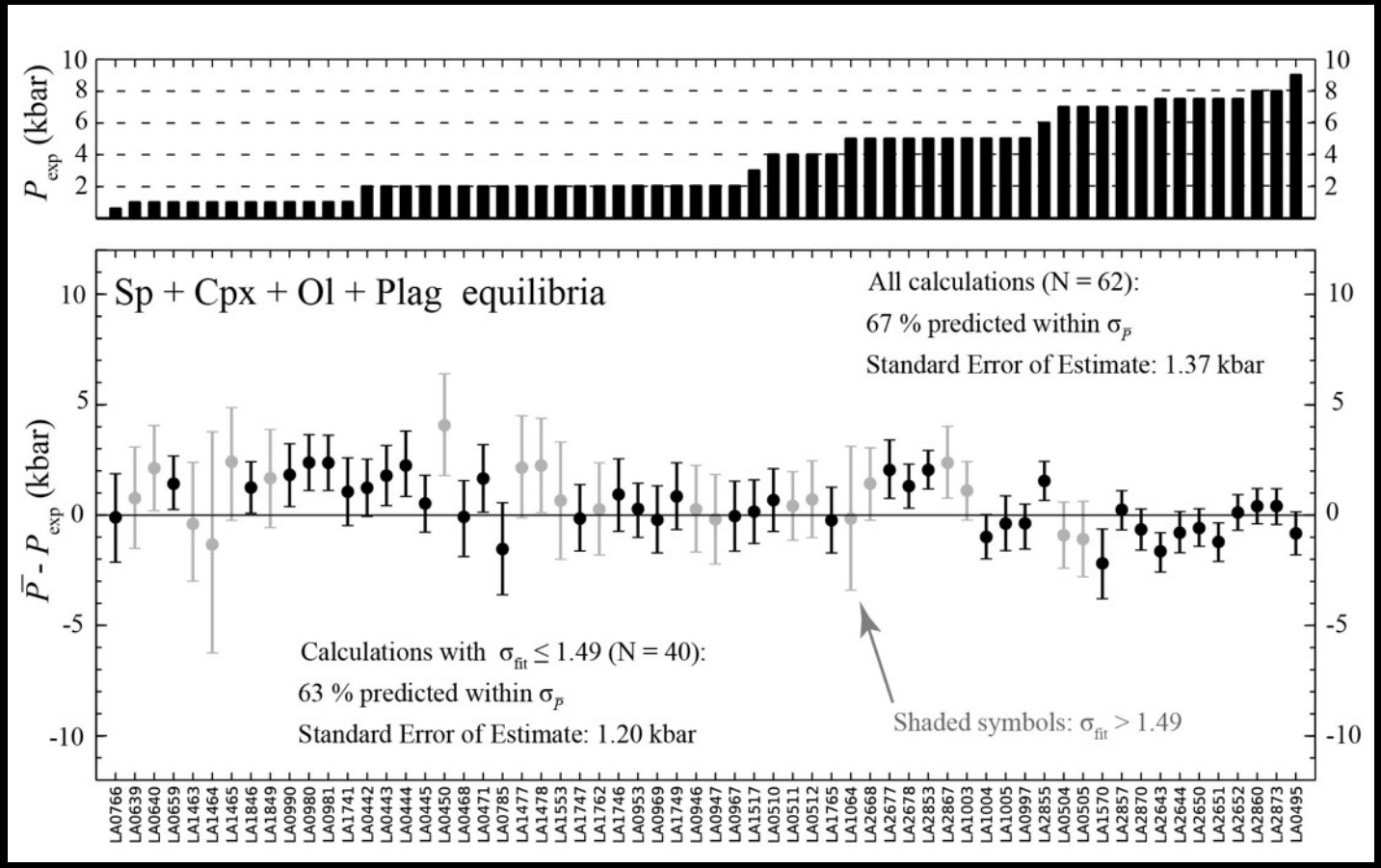


*Ziberna et al (2017, Am Min)*

# Application of avP to the experimental samples

No deviations with temperature and composition

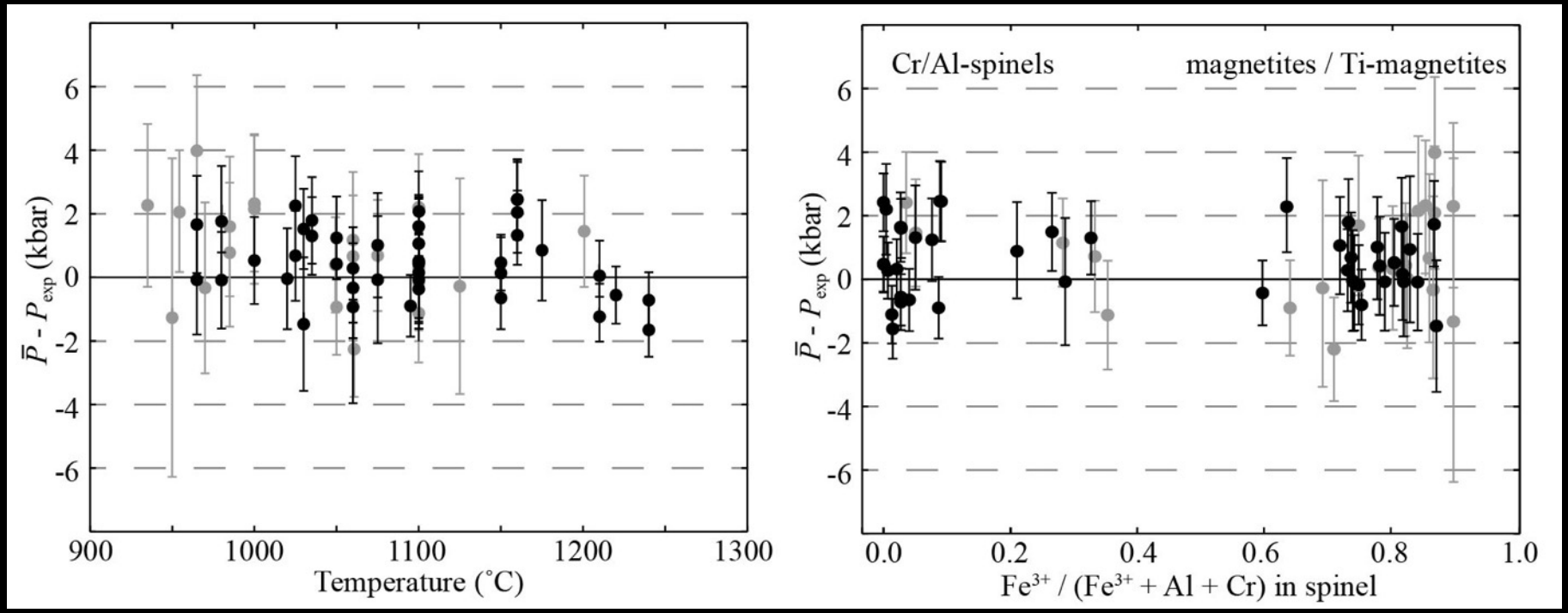


*Ziberna et al (2017, Am Min)*

# Application of avP to the xenoliths

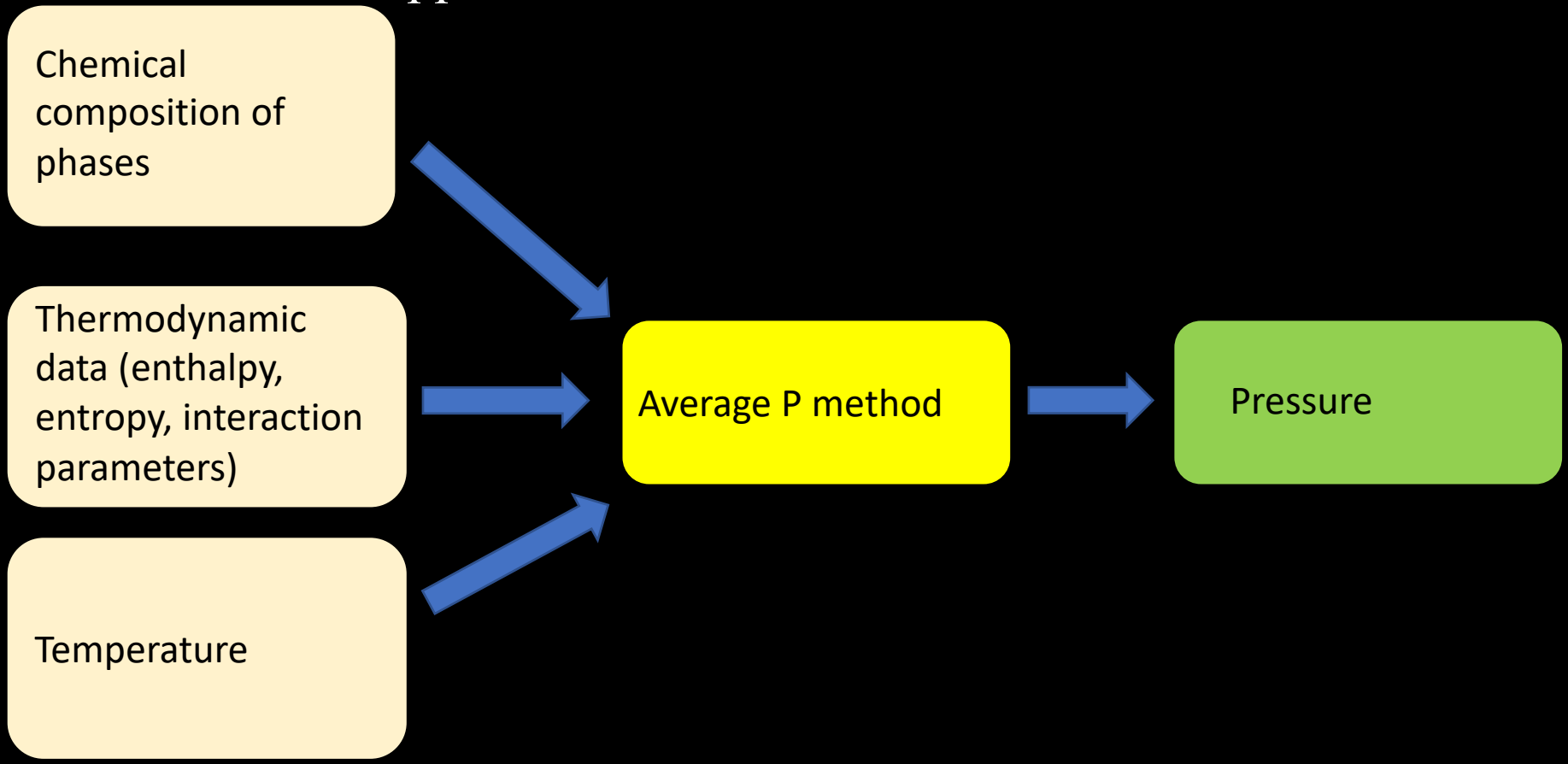

# Application of avP to the xenoliths

Chemical composition of phases

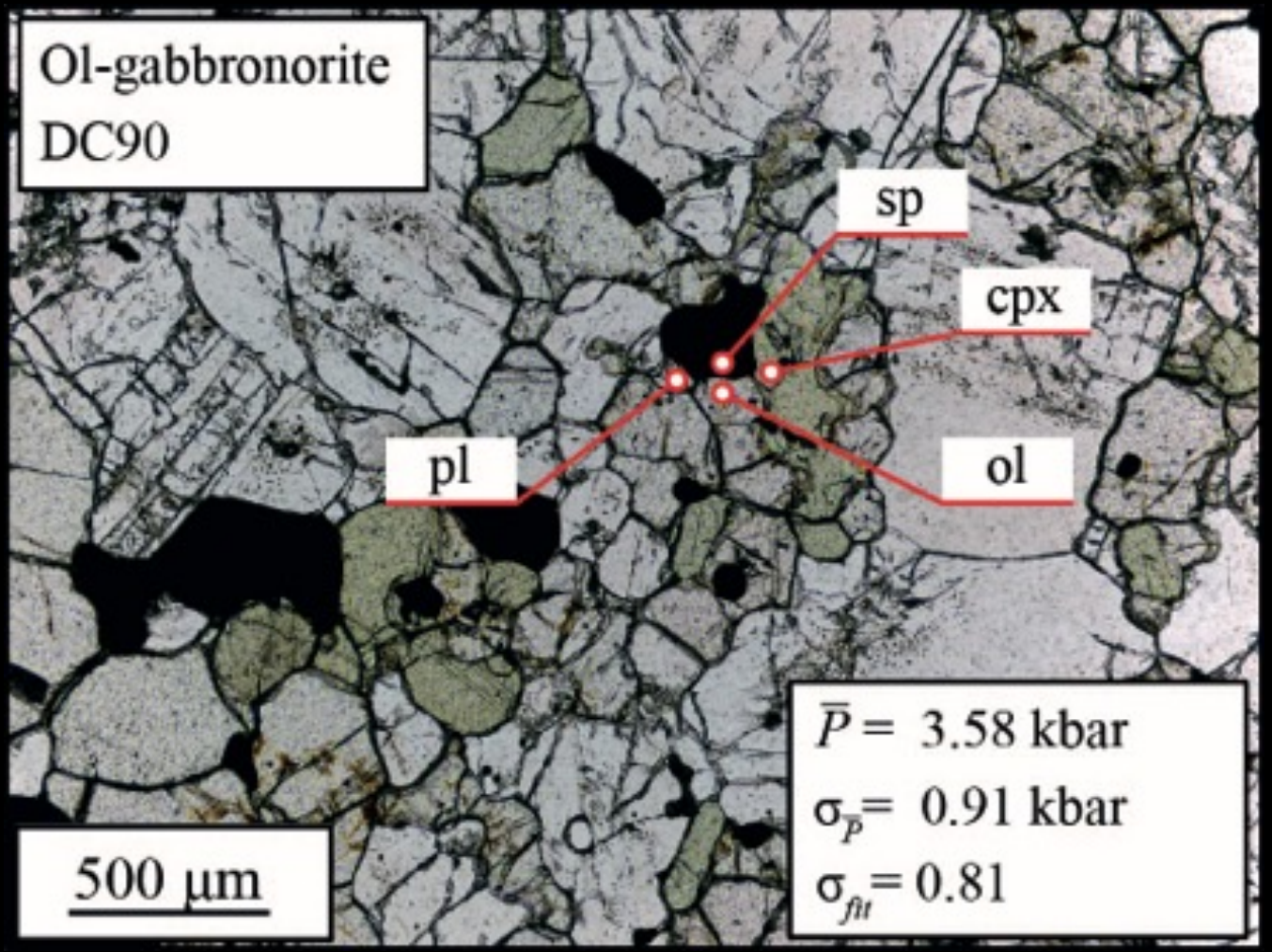

# Application of avP to the xenoliths

Thermodynamic data (enthalpy, entropy, interaction parameters)

*Holland & Powell (2011; J M G)*



**Table 2a.** Molar thermodynamic properties (units: kJ, K, kbar) of the end-members whose formulae can be found in Table 1.

| Group | End-member | $\Delta_f H$ | $\sigma(\Delta_f H)$ | $S$ | $V$ | $C_P$ | | | | $\alpha\kappa$ | | | | $\ell$ |
|---|---|---|---|---|---|---|---|---|---|---|---|---|---|---|
| | | | | | | a | b | c | d | $\alpha_0$ | $\kappa_0$ | $\kappa_0'$ | $\kappa_0''$ | |
| Garnet and olivine | Almandine (alm) | −5260.65 | 1.31 | 342.00 | 11.525 | 0.6773 | 0 | −3772.7 | −5.0440 | 2.12 | 1900.0 | 2.98 | −0.0016 | |
| | Andradite (andr) | −5769.08 | 1.56 | 316.40 | 13.204 | 0.6386 | 0 | −4955.1 | −3.9892 | 2.86 | 1588.0 | 5.68 | −0.0036 | |
| | grossular (gr) | −6642.95 | 1.46 | 255.00 | 12.535 | 0.6260 | 0 | −5779.2 | −4.0029 | 2.20 | 1720.0 | 5.53 | −0.0032 | |
| | Knorringite (knor) | −5687.75 | 3.88 | 317.00 | 11.738 | 0.6130 | 0.3606 | −4178.0 | −3.7294 | 2.37 | 1743.0 | 4.05 | −0.0023 | |
| | Majorite (maj) | −6050.33 | 9.62 | 255.20 | 11.457 | 0.7136 | −0.0997 | −1158.2 | −6.6223 | 1.83 | 1600.0 | 4.56 | −0.0028 | |
| | Pyrope (py) | −6282.13 | 1.06 | 269.50 | 11.313 | 0.6335 | 0 | −5196.1 | −4.3152 | 2.37 | 1743.0 | 4.05 | −0.0023 | |
| | Spessartine (spss) | −5693.65 | 3.14 | 335.30 | 11.792 | 0.6469 | 0 | −4525.8 | −4.4528 | 2.27 | 1740.0 | 6.68 | −0.0038 | |
| | Clinohumite (chum) | −9609.82 | 2.49 | 443.00 | 19.785 | 1.0700 | −1.6533 | −7899.6 | −7.3739 | 2.91 | 1194.0 | 4.79 | −0.0040 | |
| | Fayalite (fa) | −1477.74 | 0.68 | 151.00 | 4.631 | 0.2011 | 1.7330 | −1960.6 | −0.9009 | 2.82 | 1256.0 | 4.68 | −0.0037 | |
| | Forsterite (fo) | −2172.57 | 0.57 | 95.10 | 4.366 | 0.2333 | 0.1494 | −603.8 | −1.8697 | 2.85 | 1285.0 | 3.84 | −0.0030 | |
| | Larnite (lrn) | −2307.04 | 0.90 | 127.60 | 5.160 | 0.2475 | −0.3206 | 0 | −2.0519 | 2.90 | 985.0 | 4.07 | −0.0041 | 1 |
| | Monticellite (mont) | −2251.31 | 0.52 | 109.50 | 5.148 | 0.2507 | −1.0433 | −797.2 | −1.9961 | 2.87 | 1134.0 | 3.87 | −0.0034 | |
| | Tephroite (teph) | −1733.95 | 1.05 | 155.90 | 4.899 | 0.2196 | 0 | −1292.7 | −1.3083 | 2.86 | 1256.0 | 4.68 | −0.0037 | |
| Aluminosilicates | Andalusite (and) | −2588.72 | 0.68 | 92.70 | 5.153 | 0.2773 | −0.6588 | −1914.1 | −2.2656 | 1.81 | 1442.0 | 6.89 | −0.0048 | |
| | Kyanite (ky) | −2593.02 | 0.67 | 83.50 | 4.414 | 0.2794 | −0.7124 | −2055.6 | −2.2894 | 1.92 | 1601.0 | 4.05 | −0.0025 | |
| | Sillimanite (sill) | −2585.85 | 0.68 | 95.40 | 4.986 | 0.2802 | −0.6900 | −1375.7 | −2.3994 | 1.12 | 1640.0 | 5.06 | −0.0031 | 2 |
| | Mullite (amul) | −2485.51 | 0.91 | 113.00 | 5.083 | 0.2448 | 0.0968 | −2533.3 | −1.6416 | 1.36 | 1740.0 | 4.00 | −0.0023 | |
| | Mullite (smul) | −2569.28 | 0.69 | 101.50 | 4.987 | 0.2802 | −0.6900 | −1375.7 | −2.3994 | 1.36 | 1740.0 | 4.00 | −0.0023 | |
| | Chloritoid (fctd) | −3208.31 | 0.80 | 167.00 | 6.980 | 0.4161 | −0.3477 | −2835.9 | −3.3603 | 2.80 | 1456.0 | 4.06 | −0.0028 | |
| | Chloritoid (mctd) | −3549.31 | 0.75 | 146.00 | 6.875 | 0.4174 | −0.3771 | −2920.6 | −3.4178 | 2.63 | 1456.0 | 4.06 | −0.0028 | |
| | Chloritoid (mnctd) | −3336.20 | 1.68 | 166.00 | 7.175 | 0.4644 | −1.2654 | −1147.2 | −4.3410 | 2.60 | 1456.0 | 4.06 | −0.0028 | |
| | Staurolite (fst) | −23 755.04 | 6.34 | 1010.00 | 44.880 | 2.8800 | −5.6595 | −10642.0 | −25.3730 | 1.83 | 1800.0 | 4.76 | −0.0026 | |
| | Staurolite (mnst) | −24 246.42 | 8.60 | 1034.00 | 45.460 | 2.8733 | −8.9064 | −12688.0 | −24.7490 | 2.09 | 1800.0 | 4.76 | −0.0026 | |
| | Staurolite (mst) | −25 124.32 | 6.28 | 910.00 | 44.260 | 2.8205 | −5.9366 | −13774.0 | −24.1260 | 1.81 | 1684.0 | 4.05 | −0.0024 | |
| | Topaz (tpz) | −2900.76 | 0.96 | 100.50 | 5.339 | 0.3877 | −0.7120 | −857.2 | −3.7442 | 1.57 | 1315.0 | 4.06 | −0.0031 | |

# Application of avP to the xenoliths

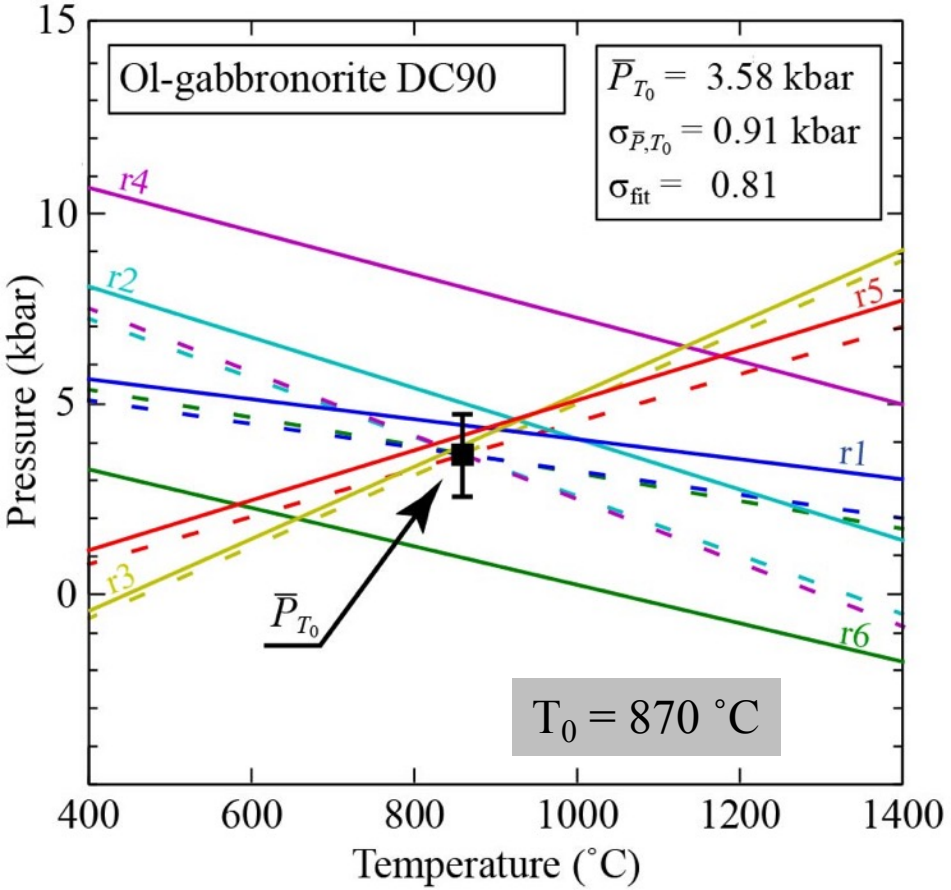


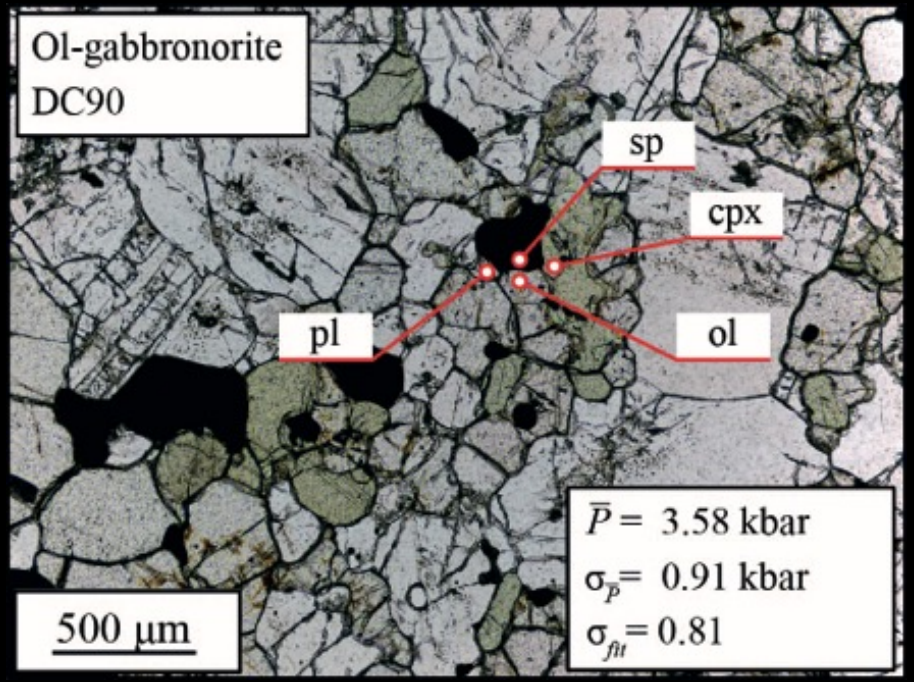


r1) $Mg_2Si_2O_6 + CaAl_2SiO_6 = Mg_2SiO_4 + CaAl_2Si_2O_8$

r2) $Fe_2Si_2O_6 + CaAl_2SiO_6 = Fe_2SiO_4 + CaAl_2Si_2O_8$

r3) $Mg_2Si_2O_6 + NaAlSi_2O_6 = Mg_2SiO_4 + NaAlSi_3O_8$

r4) $Mg_2Si_2O_6 + 2\ CaAl_2SiO_6 = CaMgSi_2O_6 + CaAl_2Si_2O_8 + MgAl_2O_4$

r5) $Mg_2Si_2O_6 + NaAlSi_2O_6 + 2\ FeAl_2O_4 = Fe_2SiO_4 + NaAlSi_3O_8 + 2\ MgAl_2O_4$

r6) $2\ Fe_2Si_2O_6 + 2\ NaFeSi_2O_6 + FeAl_2O_4 = 2\ Fe_2SiO_4 + 2\ NaAlSi_3O_8 + Fe_3O_4$

# Application of avP to the xenoliths

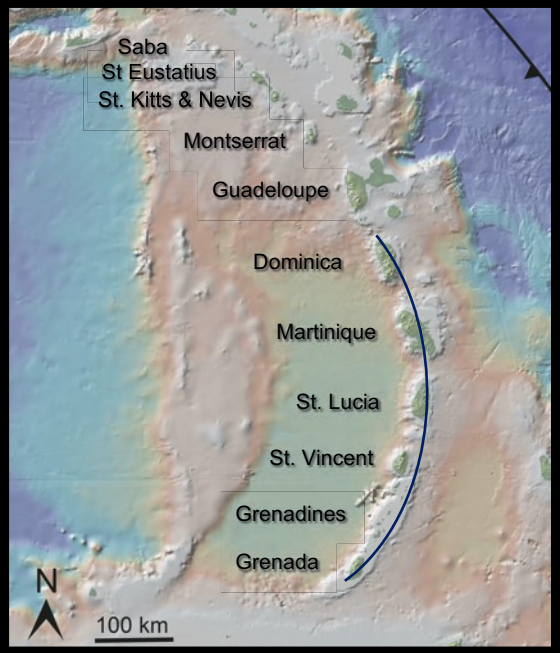


## Along-arc variations

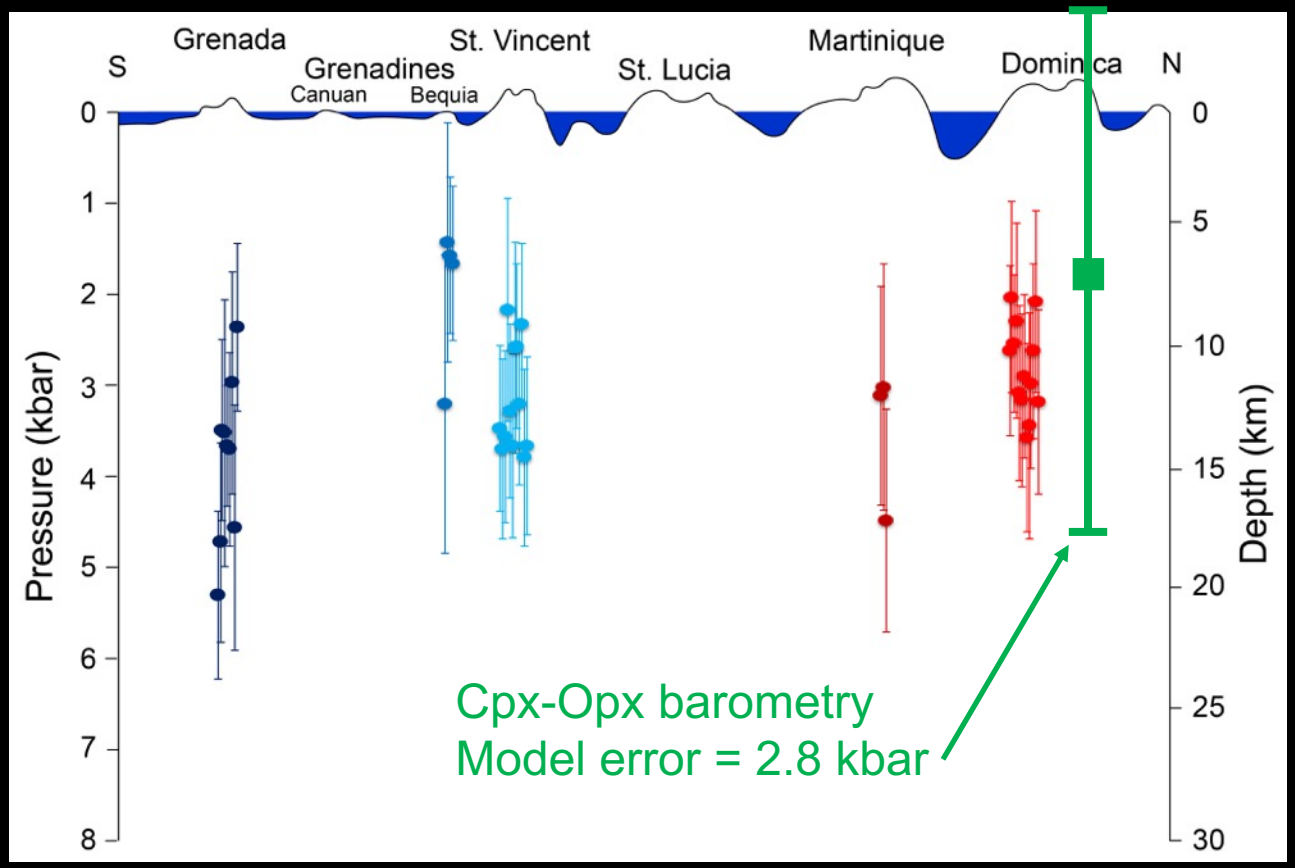

# Application of avP to the xenoliths

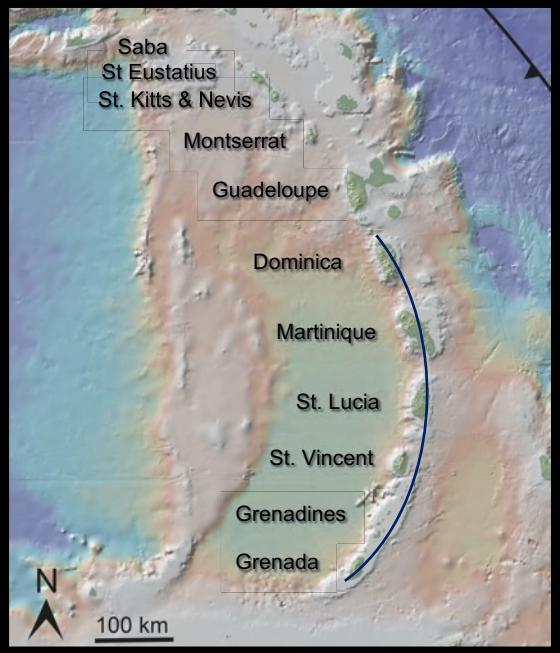


## Variations of petrological variables with depth

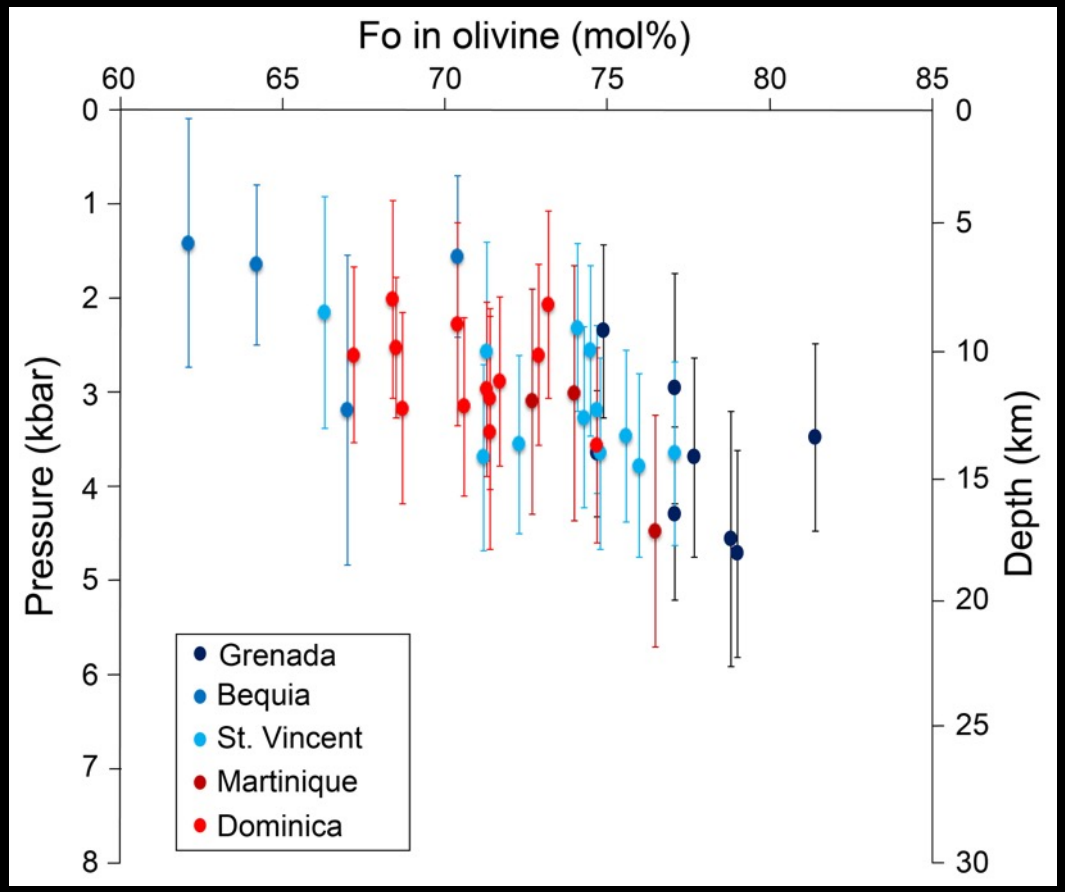

# Integration with seismic models

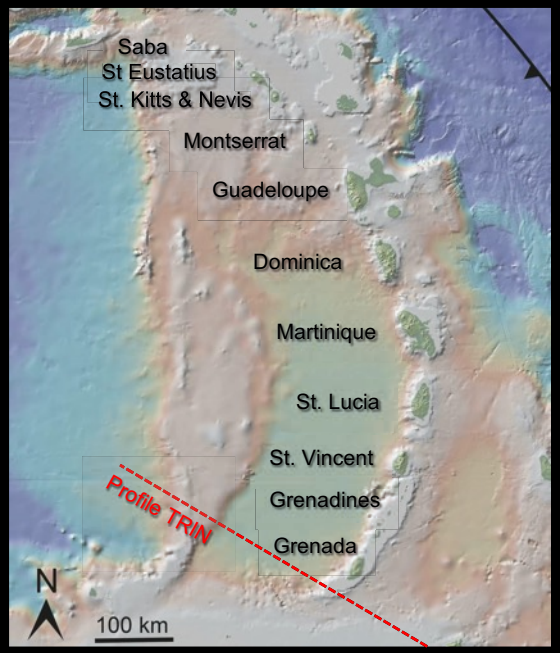


Calculated seismic properties (using Hacker & Abers, 2004)

Grenada xenoliths:

ρ (density) = 2.84 – 3.20 g/cm$^3$

**Vp (P wave velocity) = 6.63 – 7.58 km/s**

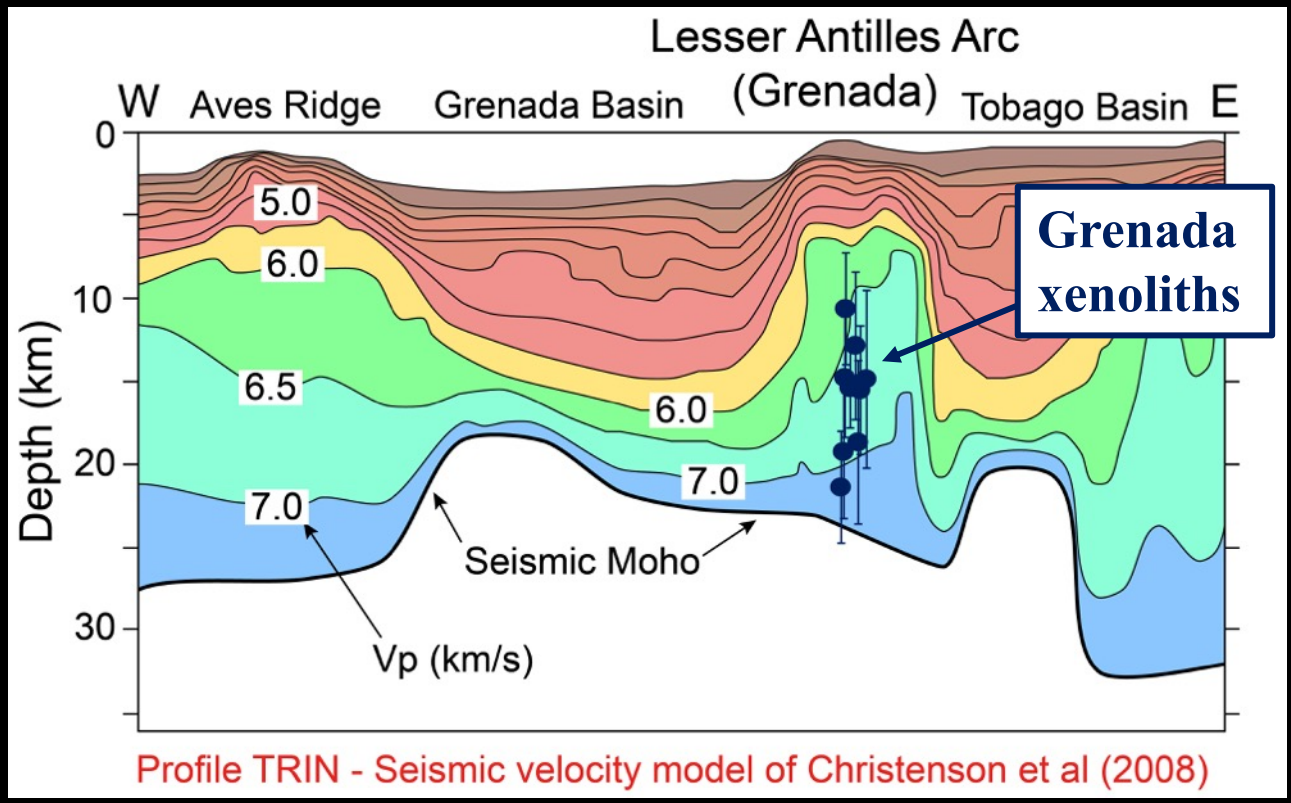

# Integration with seismic models

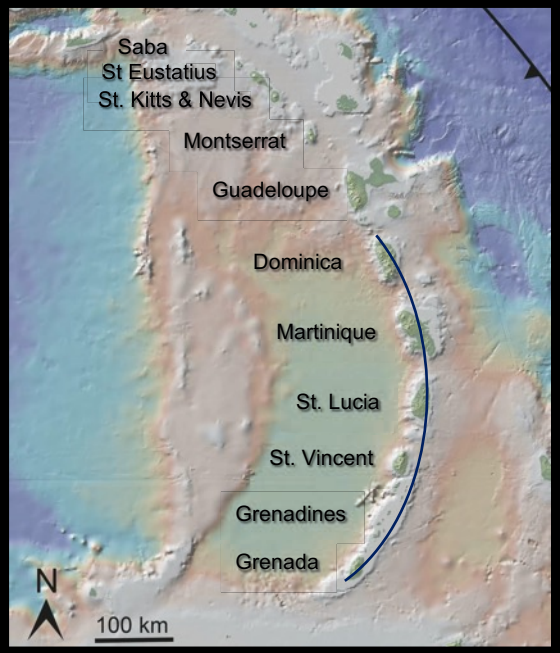


Lesser Antilles (Grenada)

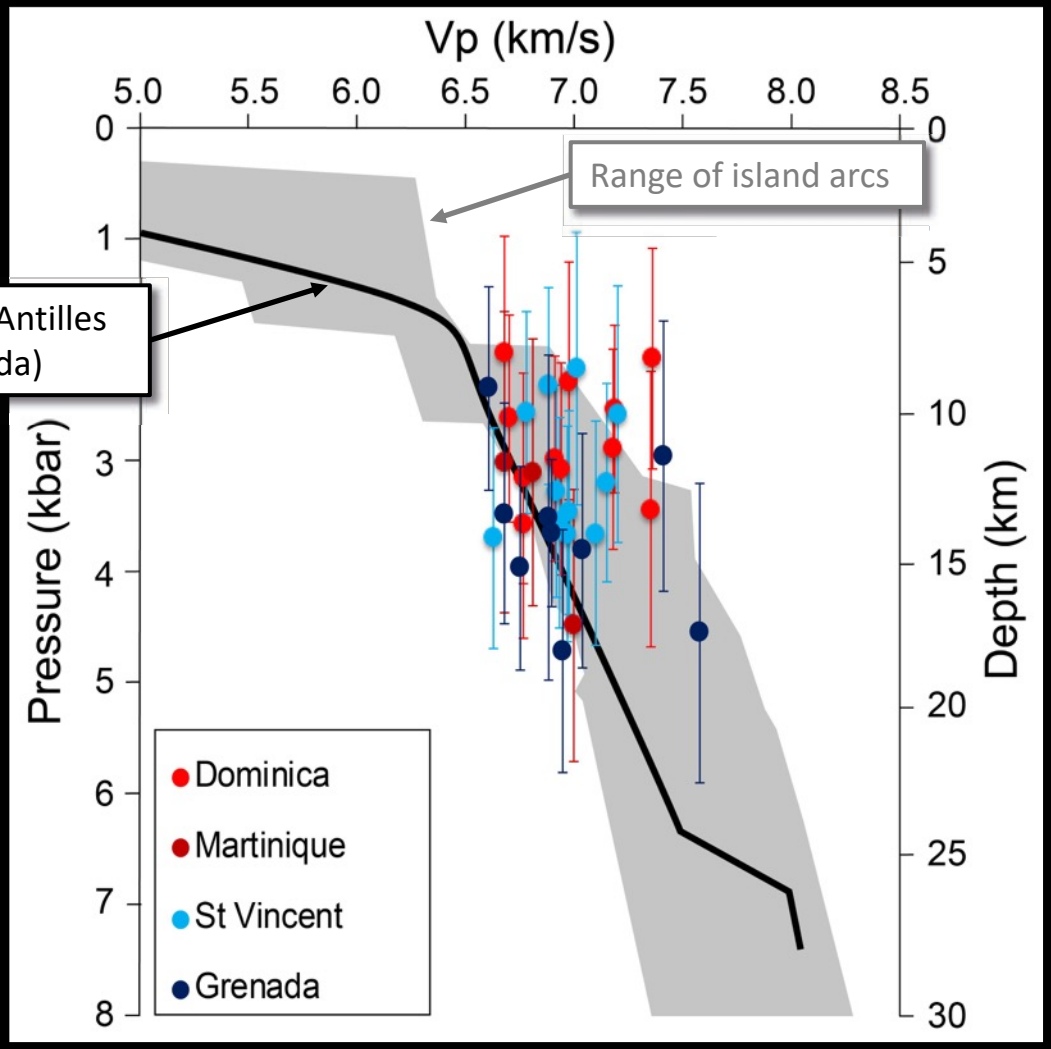

# Modelli termodinamici diretti

La modellizzazione termodinamica diretta viene utilizzata per predire come la mineralogia e le proprietà chimico-fisiche delle rocce e dei magmi variano in funzione delle condizioni (P, T, $fO_2$, etc).

I principi su cui si basa sono gli stessi della termobarometria classica.

I software di modellizzazione termodinamica più utilizzati in petrologia sono:

- MELTS (http://melts.ofm-research.org/index.html)

- PERPLE_X (http://perplex.ethz.ch)

- THERMOCALC (http://www.metamorph.geo.uni-mainz.de/thermocalc/)

# Esempio di studio

Contrib Mineral Petrol (2016) 171:16
DOI 10.1007/s00410-016-1229-9

CrossMark

ORIGINAL PAPER

## Application of thermodynamic modelling to natural mantle xenoliths: examples of density variations and pressure–temperature evolution of the lithospheric mantle

L. Ziberna[1] · S. Klemme[2]

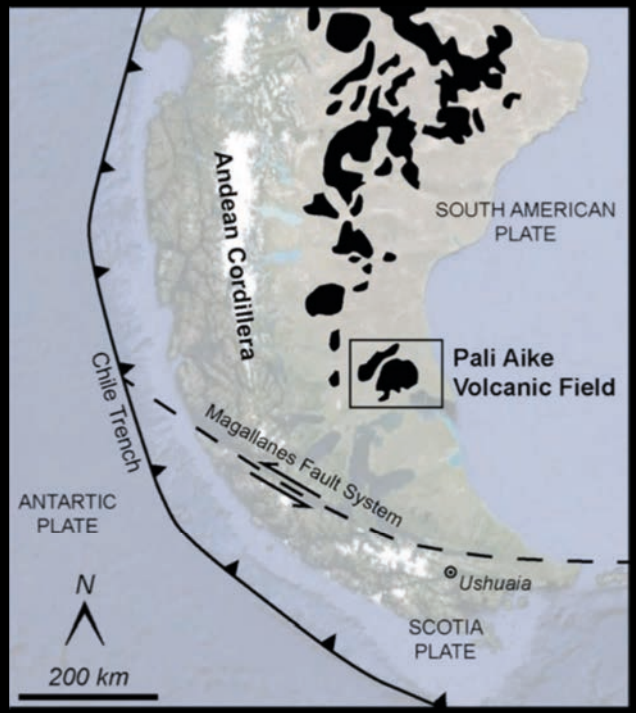


# Esempio di studio

**Table 1** Bulk compositions for which phase relations were calculated in this study

| | LS1 | | PA3 | | LS2 | | TM16 | |
|---|---|---|---|---|---|---|---|---|
| | Spinel harzburgite | | Spinel harzburgite | | Spinel harzburgite | | Spinel–garnet harzburgite | |
| | Whole-rock[a] | Model[b] | Whole-rock[a] | Model | Whole-rock[c] | Model | Whole-rock[a] | Model |
| $SiO_2$ | 43.31 | 43.74 | 43.95 | 44.53 | 42.11 | 42.66 | 47.34 | 47.52 |
| $TiO_2$ | 0.04 | – | 0.05 | – | 0.03 | – | 0.23 | – |
| $Al_2O_3$ | 0.52 | 0.53 | 1.03 | 1.04 | 3.55 | 3.60 | 3.27 | 3.28 |
| $Cr_2O_3$ | 0.34 | 0.34 | 0.46 | 0.47 | 0.82 | 0.83 | 0.37 | 0.37 |
| $FeO_{tot}$ | 6.80 | 6.87 | 7.58 | 7.68 | 9.03 | 9.15 | 8.73 | 8.76 |
| MnO | 0.10 | – | 0.12 | – | 0.11 | – | 0.13 | – |
| MgO | 47.64 | 48.12 | 44.86 | 45.46 | 41.94 | 42.48 | 39.06 | 39.21 |
| CaO | 0.40 | 0.40 | 0.79 | 0.80 | 1.23 | 1.25 | 0.81 | 0.81 |
| $Na_2O$ | 0.00 | 0.00 | 0.02 | 0.02 | 0.04 | 0.04 | 0.05 | 0.05 |
| $K_2O$ | 0.00 | – | 0.02 | – | n.a. | – | 0.09 | – |
| NiO | 0.33 | – | 0.32 | – | 0.24 | – | 0.24 | – |
| Mg# | 0.93 | 0.93 | 0.91 | 0.91 | 0.89 | 0.89 | 0.89 | 0.89 |
| Cr# | 0.30 | 0.30 | 0.23 | 0.23 | 0.13 | 0.13 | 0.07 | 0.07 |
| Ca# | 0.01 | 0.01 | 0.01 | 0.01 | 0.02 | 0.02 | 0.01 | 0.01 |

Composizione chimica utilizzata come input per il modello

| | LS1 | |
|---|---|---|
| | Spinel harzburgite | |
| | Whole-rock[a] | Model[b] |
| $SiO_2$ | 43.31 | 43.74 |
| $TiO_2$ | 0.04 | – |
| $Al_2O_3$ | 0.52 | 0.53 |
| $Cr_2O_3$ | 0.34 | 0.34 |
| $FeO_{tot}$ | 6.80 | 6.87 |
| MnO | 0.10 | – |
| MgO | 47.64 | 48.12 |
| CaO | 0.40 | 0.40 |
| $Na_2O$ | 0.00 | 0.00 |
| $K_2O$ | 0.00 | – |
| NiO | 0.33 | – |
| Mg# | 0.93 | 0.93 |
| Cr# | 0.30 | 0.30 |
| Ca# | 0.01 | 0.01 |

# Esempio di studio

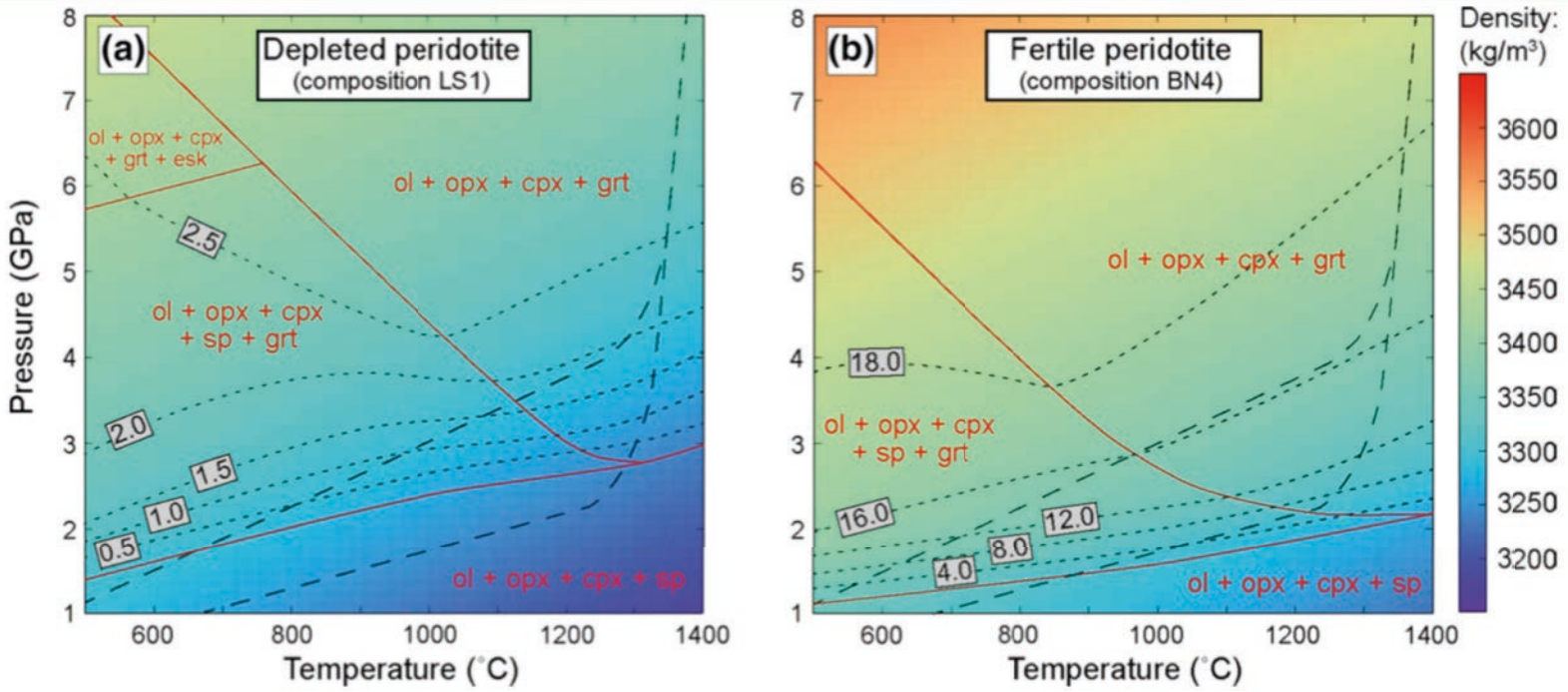


**Fig. 3** Pressure–temperature diagram showing a colour map of the calculated density for the compositions **a** LS1 and **b** BN4 (mantle xenoliths from Pali-Aike, Stern et al. 1999). The two dashed curves represent a 50 (*higher curve*) and a 70 mW/m$^2$ (*lower curve*) conductive geotherms both joining the 1300 °C adiabat (Hasterok and Chapman 2011). The solid red curves delimit the stability fields predicted by the thermodynamic model (*ol* olivine, *opx* orthopyroxene, *cpx* clinopyroxene, *grt* garnet, *sp* spinel, *esk* eskolaite). It is worth noting that garnet modes (*isopleths marked by grey squares*) have the major control on density variations across the spinel–garnet transition. The smoother density variation at the spinel–garnet transition in (**a**) is indeed related to the very low modes of garnet (<3.0 wt%) for composition BN4 (see text)

# Esempio di studio

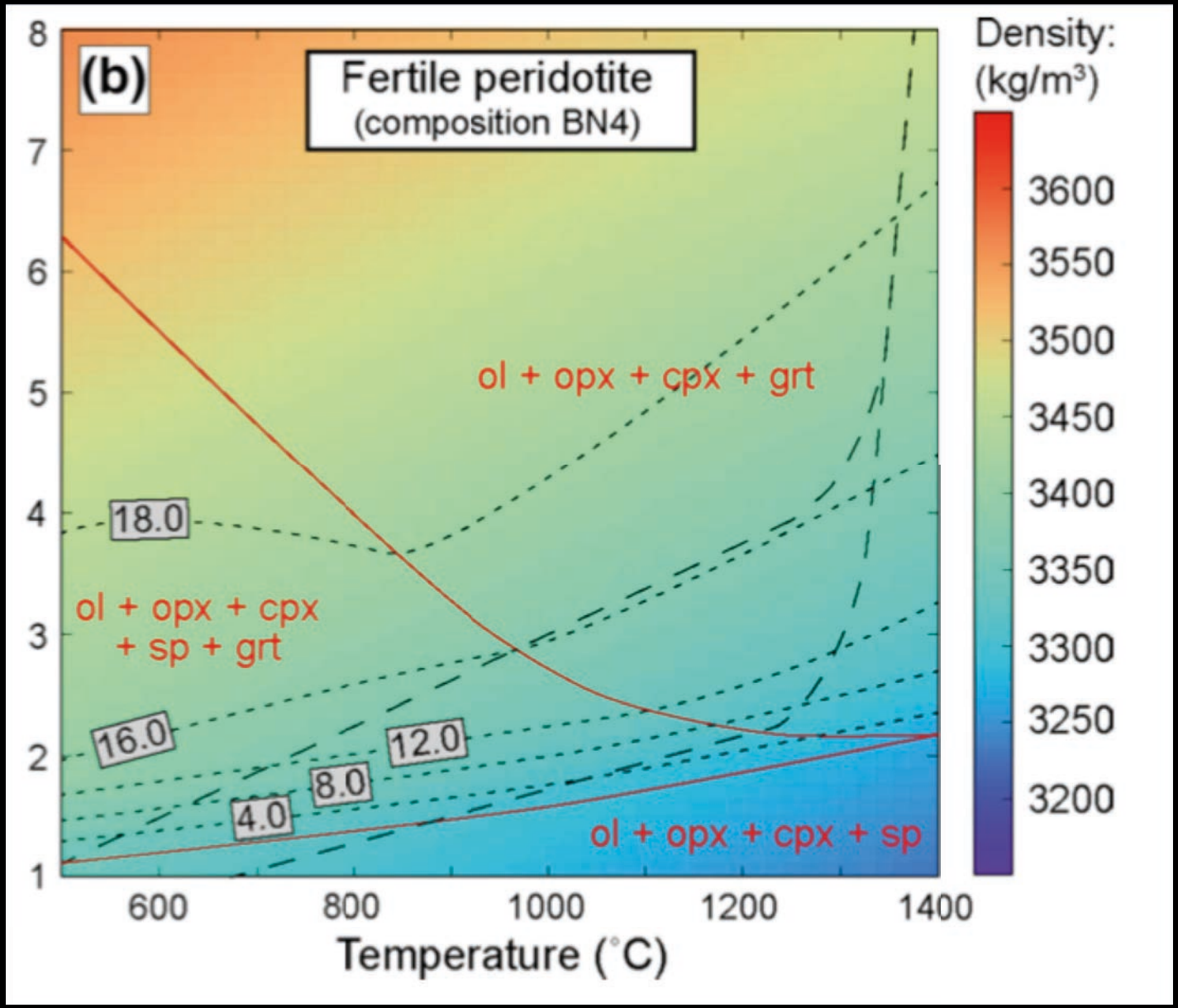

# Esempio di studio

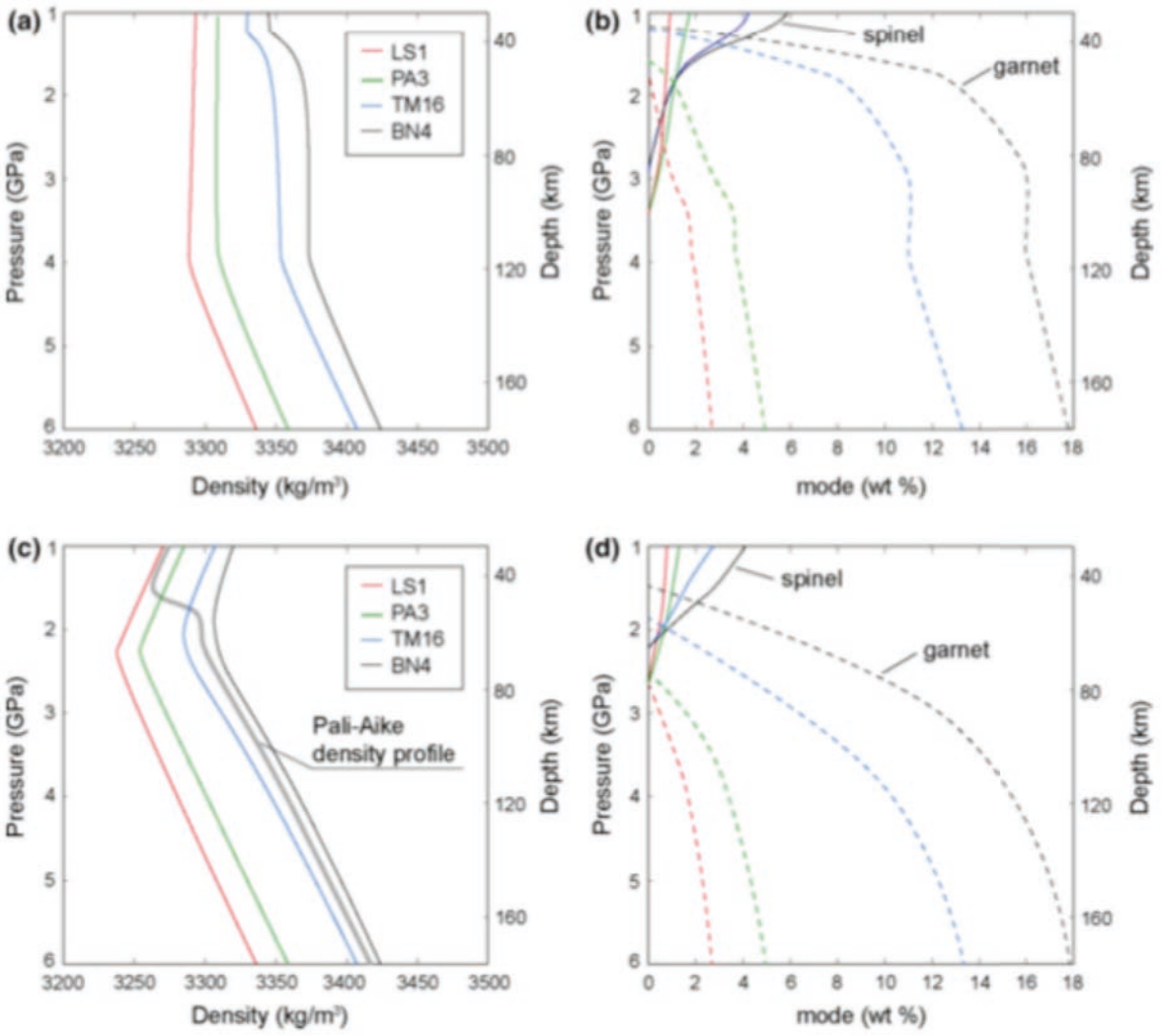


**Fig. 4** Calculated density profiles and garnet (*dashed lines*) and spinel (*solid lines*) modes for some representative Pali-Aike peridotite compositions (Table 1) along a 50 mW/m$^2$ steady state geotherm (**a**, **b**) and a 70 mW/m$^2$ geotherm (**c**, **d**). The *solid grey curve* in (**c**) represents a possible density profile beneath Pali-Aike based on the compositional layering observed by (Stern et al. 1999). For sake of simplicity, the depth values shown on the right axes were calculated assuming constant density (i.e. depth = P(GPa) 9.8 m/s$^2$ · 3.0 kg/cm$^3$)

# Esempio di studio

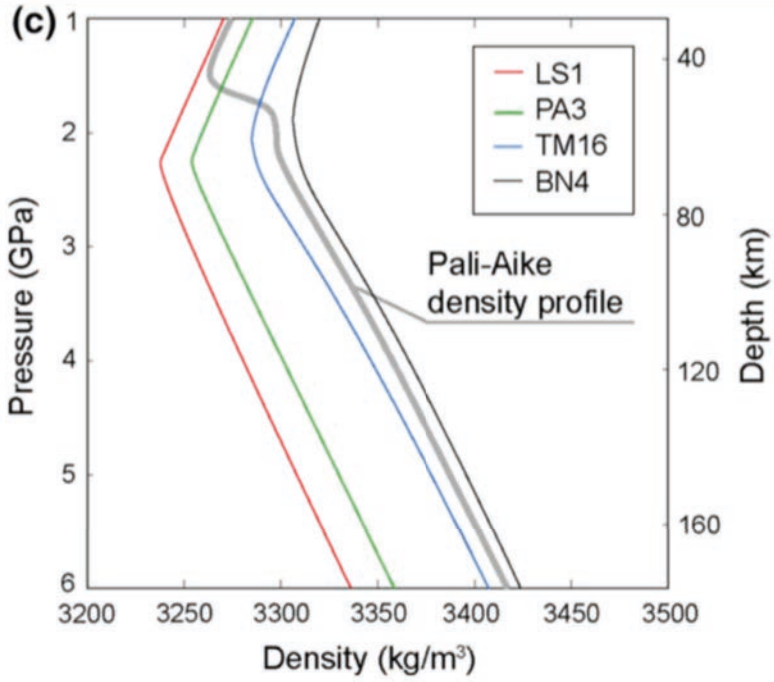


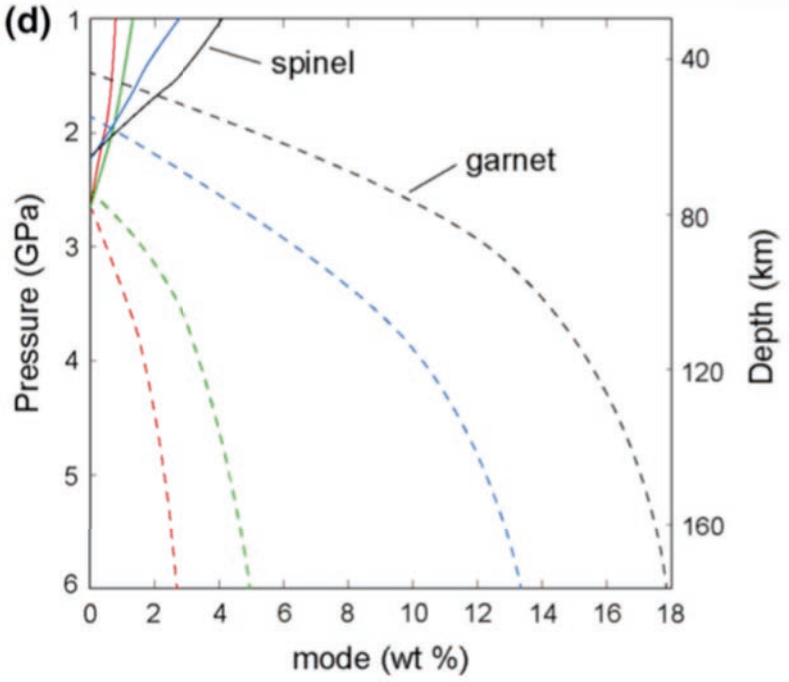


**Fig. 4** Calculated density profiles and garnet (*dashed lines*) and spinel (*solid lines*) modes for some representative Pali-Aike peridotite compositions (Table 1) along a 50 mW/m$^2$ steady state geotherm (**a**, **b**) and a 70 mW/m$^2$ geotherm (**c**, **d**). The *solid grey curve* in (**c**) represents a possible density profile beneath Pali-Aike based on the compositional layering observed by (Stern et al. 1999). For sake of simplicity, the depth values shown on the right axes were calculated assuming constant density (i.e. depth = P(GPa) 9.8 m/s$^2$ · 3.0 kg/cm$^3$)

# Esempio di studio con MELTS

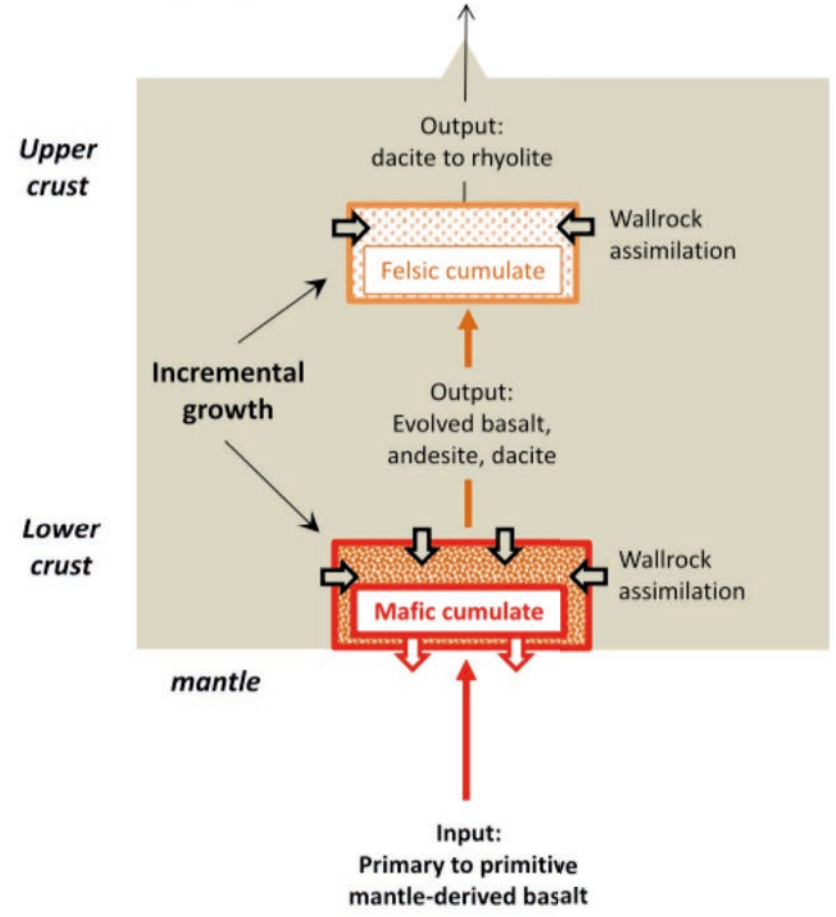


**Fig. 7.** Cartoon showing polybaric multi-stage differentiation history of magmas. Primary, mantle derived basalts rise from the mantle and stall in or below the deep crust, resulting in cooling, crustal assimilation and crystal fractionation. This generates a range of compositions from evolved basalts to dacites, depending on conditions, such as water content. Andesites dominate in continental arc settings. Such melts then rises into the middle and upper crust, where they differentiate by crystal–liquid segregation to form rhyolitic liquids. Mixing can occur anywhere along this path due to the incremental growth of reservoirs, but is not crucial to the generation of intermediate magmas.

# Esempio di studio con MELTS

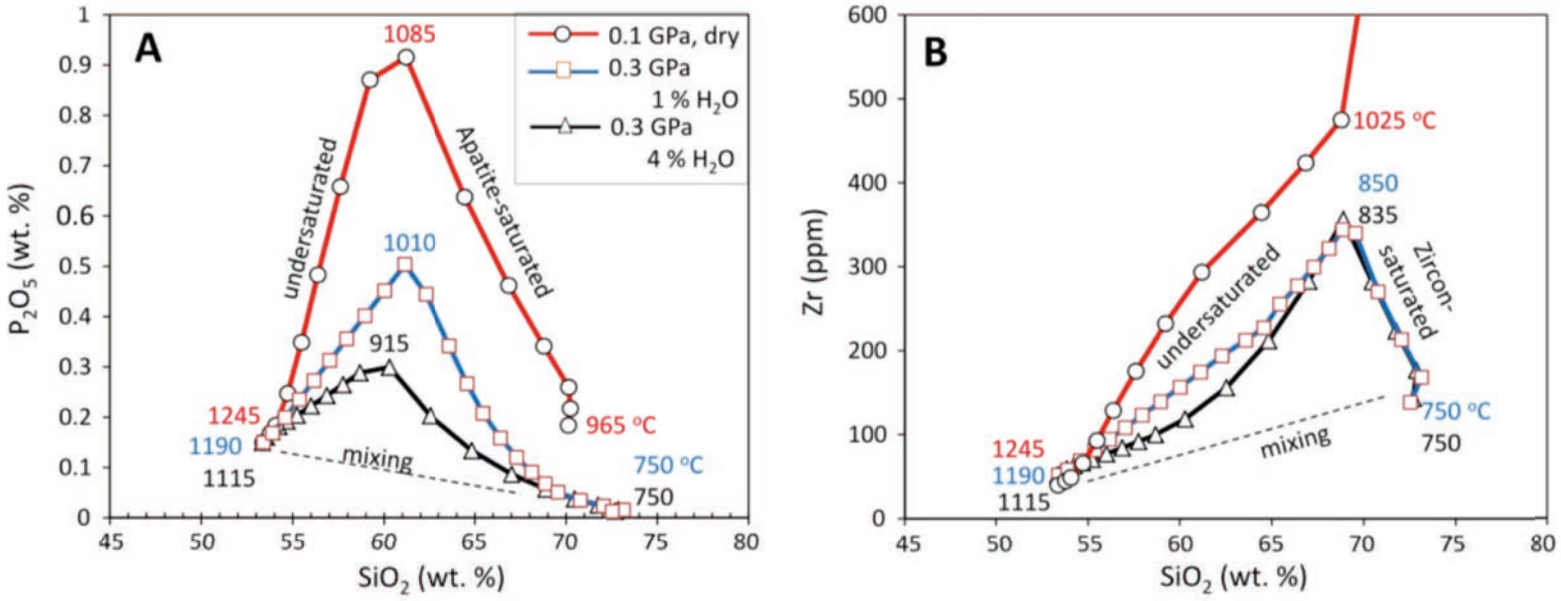


**Fig. 2.** Modeled residual liquids formed by equilibrium crystallization of dry and hydrous parental basalts using Rhyolite-Melts (Gualda et al., 2012). $P_2O_5$ (wt.%) and Zr (ppm) are plotted against $SiO_2$ (wt.%) in (a) and (b), respectively. Elemental concentrations have been normalized to a volatile-free system. Temperatures at the liquidus, point of saturation in apatite or zircon, and the solidus are shown for reference. Dashed straight line in (a) and (b) are hypothetical mixing lines.

# Esempio di studio con MELTS